Research Article

Robin De Schryver* and Geert De Schutter

Insights in thixotropic concrete pumping by a Poiseuille flow extension

https://doi.org/10.1515/arh-2020-0103
Received Apr 16, 2020; accepted Jul 24, 2020

Abstract: Thixotropy is a reversible time-dependent phenomenon in fluids, in which an internal structure grows due to flocculation and breaks down under shear action. Numerous fluids are thixotropic, *e.g.* concretes and cementitious suspensions. Pumping of concrete is an important application. Since current approaches omit thixotropic effects, we aim to develop a simple theoretical model to evaluate or understand the significance of thixotropy on the concrete pumping behaviour. We therefore extended Poiseuille flow for thixotropic concretes and reformulated it in a dimensionless form to gain insights. After a validation, the results and significance are elaborated and concluded.

Results showed that for increasing thixotropy and decreasing flow rates, the plug radius, wall shear rate and pumping pressure loss increase. Even though all thixotropy mechanisms may not be covered, a simple model is delivered to interpret or predict the effect of thixotropy on the pumping behaviour of cementitious suspensions. The dimensionless formulations via the Bingham number Bn and related discharge diagrams are sufficiently elegant for computational implementation and very insightful to distinguish a thixotropic flow regime. The model could be extended for more complicated thixotropies, irreversible time-dependent effects or even other pumping related phenomena.

Keywords: Thixotropy, Pumping, Poiseuille flow, Concrete rheology, Bingham number

***Corresponding Author: Robin De Schryver:** Magnel-Vandepitte Laboratory, Department of Structural Engineering and Building Materials, Faculty of Engineering and Architecture, Ghent University, Technologiepark-Zwijnaarde 60, B-9052 Ghent, East Flanders, Belgium; Email: Robin.DeSchryver@UGent.be
Geert De Schutter: Magnel-Vandepitte Laboratory, Department of Structural Engineering and Building Materials, Faculty of Engineering and Architecture, Ghent University, Technologiepark-Zwijnaarde 60, B-9052 Ghent, East Flanders, Belgium

1 Introduction

Thixotropy is a reversible time-dependent effect that is present in many fluids and related applications [1]. Depending on the field of application, thixotropy has different definitions [1–5]. Barnes [1] states that thixotropy is a reversible time-dependent effect leading to an increase in flow resistance at rest and a decrease in viscosity under shear action. One could summarise thixotropy as a reversible time-dependent change in apparent viscosity (flow resistance), due to formation of an internal structure by flocculation at rest and deflocculation under shear action [2, 3]. Several models exist that try to characterise thixotropic behaviour in rheology, *i.e.* the study of material stresses induced by applied deformation rates. Most thixotropic models describe an internal fluid structural state, either explicitly or implicitly [2–4, 6–8]. Implicit thixotropic models describe the evolution of the internal structural state by a kinematic relation. Again, several kinematic evolution relations exist and, whether a memory convolution is used or not, they can be summarised by a growth (build-up) and break-down of the internal structure [6].

Thixotropy occurs in, for example, coatings, paints, inks, crude oil suspensions, clay suspensions, creams, pharmaceutical products, food industry liquids, fresh concretes, etc. [1, 9, 10]. Pumping of these fluids is one of its major applications. Rheological predictions or understanding of the pumping behaviour of these thixotropic fluids is therefore important to industry. In the field of concrete technology, it is however often stated that thixotropy can be neglected for short duration and/or under (high) shear action. In that way, one states that thixotropic build-up is negligible, which is the case for some thixotropic models (*e.g.* the model proposed by Papo [11]). It can however be quite the opposite.

Thixotropy can have a significant influence on short duration or even under shear action [2, 6, 12, 13]. In the case of fluid/concrete pumping, it is one of the most contributing factors of pumping initiation. When structural build-up is a dominant factor such as for thixotropic concretes, pumping re-initiation pressures after pumping ar-

rests are predominantly determined by thixotropic build-up [14]. Pumping arrests are for instance common on concrete construction sites, where pumping operations need to be stopped regularly or unexpectedly [14]. Another example where build-up can be significant is the plug correction in rheological measurements (*e.g.* concentric cylinders), because an unsheared part of the rheological geometry may exist for yield stress fluids such as concrete [15, 16]. Thixotropy can influence the effect of such an unsheared zone even more due to structural build-up.

Hence, apart from break-down, thixotropic build-up effects can have a significant influence on the pumping behaviour in the concrete industry where a simple evaluation model is missing. Even though a semi-analytical solution exists for the Moore or the Houska model [17, 18], these models are not employed for fresh concrete and do not include a closed expression to evaluate the significance of thixotropy on the concrete pumping behaviour. Hence the need to develop a simple theoretical model to evaluate, understand or predict the significance of thixotropy on the concrete pumping behaviour.

We therefore made an attempt to derive a simple theoretical analytical model for thixotropic concrete pumping, not only to gain understanding in the significance of thixotropy, but also to predict thixotropic pumping behaviour. The derived model is a Poiseuille flow extension for thixotropic concretes. A general, but simple thixotropic rheological model commonly used for concrete is considered to derive the analytical solution [2]. This work thus focuses on, but is not necessarily limited to, the application of fresh concrete pumping. The derived model and insights are also relevant for any field dealing with pumping of thixotropic fluids, where the applied thixotropy model should not necessarily be the same.

First, a concise derivation is outlined of the Poiseuille flow extension for a thixotropic model commonly applied to fresh concrete. Then, dimensionless formulations are outlined providing insights and elegance for numerical implementation. The next section is dedicated to verifying the developed model, not only step-by-step, but also by comparing it with the solution for a Bingham fluid in case thixotropy is insignificant. Then, the model applicability and significance are outlined for the aimed application of thixotropic fresh concrete pumping. After that, the results of this model are interpreted in a summary and discussion section. Lastly, this work is concluded by some brief statements with regard to the derived extension.

2 Thixotropic Poiseuille Flow Extension

This section elaborates on the Poiseuille flow extension for a thixotropic fresh concrete. Poiseuille flow is characterised by flow in a pipe geometry. This flow configuration is named after the original developers, Hagen and Poiseuille [19], who developed an analytical solution in steady-state for a Newtonian fluid. A similar approach is followed in order to find an analytical solution for a thixotropic rheological model in steady-state.

Typically a relation between pressure loss, flow rate and rheological properties is obtained for the pipe flow. In order to come up with a theoretical relation, some assumptions have to be made on the occurring flow situation. To derive such a relation for a thixotropic fluid, the following assumptions are imposed with a corresponding pipe flow configuration depicted in Figure 1:

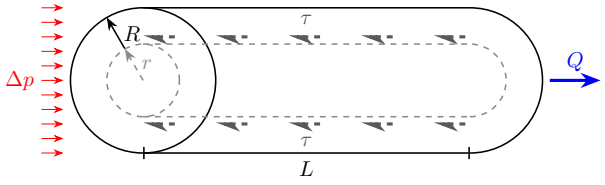

Figure 1: Poiseuille pipe flow configuration expresses a longitudinal force equilibrium between pressure loss Δp and internal shear stress τ as a function of pipe radius r.

- The fluid is incompressible and homogeneous.
- The flow is isothermal, laminar, one-dimensional and steady-state.
- There is no wall slippage and no lubrication layer formation.

with :

τ	:	Shear stress
Δp	:	Pressure loss
Q	:	Discharge
L	:	Pipe length
R	:	Pipe radius
r	:	Radial coordinate

Wall slippage is not considered in this work, as this is one of the basic assumptions in Poiseuille flow. In reality, wall slippage is not expected to be present in case of cementitious paste suspensions or even mortars and concrete, *e.g.* self-compacting concrete [20–23]. Even if wall slippage would occur, still, the flow behaviour for

a thixotropic bulk can be anticipated via an adopted approach as done by [21]. Hence, this work is still of value for both cementitious suspensions and concrete itself.

From these assumptions and notations, the derivation of the analytical solution to Poiseuille flow can be obtained as follows. First, a shear stress profile is achieved from the longitudinal force equilibrium. Secondly, a shear rate relation is established from the considered rheological model, which is in this work a thixotropic model. Thirdly, a velocity profile is derived from this shear rate profile. Lastly, a discharge relation is derived by a flux integration. The equations in this work were partially derived manually and partially with the aid of an analytical software called Maple®. All formulated equations have been verified by the same software. For computational reasons, the developed equations were implemented in a Python program.

2.1 Shear Stress Relation

The longitudinal force equilibrium easily leads to shear stress Eq. (1). This implies a fully developed state (*i.e.* steady-state). It is well known in literature [19] that this relation is linear as a function of the pipe radius r, which is zero in the pipe centre and $\tau_w = \frac{R\Delta p}{2L}$ at the pipe wall.

$$\tau(r) = \frac{r}{2}\frac{\Delta p}{L} \tag{1}$$

2.2 Shear Rate Relation

A shear rate $\dot{\gamma}$ relation can be found by inverting the shear stress relation. Therefore, a constitutive rheological material model needs to be imposed. In this framework we opt for finding a steady-state relation for a thixotropic Poiseuille flow applicable to fresh concrete. Even though a semi-analytical solution exists for the Moore or the Houska model [17, 18], these models are not applied to fresh concrete which is the aimed application in this work. The solution of the latter models is semi-analytical and therefore it is not simple. Moreover, the latter models do not contain a closed analytical expression for the pumping pressure prediction, which is the aim of this work. Hence, a different rheological model is chosen, which is applicable to thixotropic concretes or cementitious suspensions.

Fresh concrete is commonly considered as a Bingham fluid, in which the yield stress τ_0 and plastic viscosity μ are the rheological parameters. Although several thixotropic rheological models exist for fresh concrete with a Bingham model as base model [2–4, 6–8], one useful model for thixotropic concrete is picked in particular. Namely, the model proposed by Roussel [2] is chosen, because it is a general, but simple, model applicable to fresh thixotropic concretes. Although fresh concrete is the aimed application, it may be applied to other thixotropic fluids where the same thixotropic model can be used.

Thixotropy in this model can be described by an internal structure λ, which is characterised by a kinematic evolution considering two additional rheological parameters, namely the characteristic flocculation time T and the defloccuation rate α. For fresh concrete it is shown that the model proposed by Roussel [2] simplifies to Eq. (2), because shear thickening is mostly not significant [15, 20].

$$\begin{cases} \tau &= (1+\lambda)\,\tau_0 + \mu\dot{\gamma} \\ \frac{\mathrm{D}\lambda}{\mathrm{D}t} &= \frac{1}{T} - \alpha\dot{\gamma}\lambda \end{cases} \tag{2}$$

For some concretes shear thickening can be significant which can be included by the modified Bingham model or a Herschel-Bulkley model. However, since shear thickening effects have already been incorporated in the Poiseuille flow extension derived by Feys et al. [20, 24, 25] or Thichko [26], and since the aim of this work is the effect of thixotropy, only the thixotropy is considered for interpretation in this work. Therefore, this work serves as a descriptive for thixotropy as an independent phenomenon to which the effects of shear thickening could presumably be superimposed.

In some literature fields, thixotropy is described by a normalised structure parameter λ between 0 and 1. The thixotropic state for some suspensions (*e.g.* polymeric ones) will reach a final, limited gelled structure by a unity parameter. This is not the case for cementitious suspensions or concrete. Instead, due to physiochemical mechanisms in cementitious suspensions (*e.g.* coagulation, hydration, etc.), the reversible thixotropically bound structures keep on building up over time. After a certain time span ca. 60-120 min, which depends on the type of cement and composition, the structural build-up becomes irreversible due to hydration products and permanent cluster formations. Then also irreversible effects need to be taken into account and the model proposed by Perrot would be more appropriate [27]. Hence the concrete continues to build up until it is completely hardened to an irreversible solid state after a long time period ($\lambda \to \infty$). Therefore a non-normalised kinematic equation is commonly used for cementitious suspensions and concrete, cf. [2, 4, 5, 12]. Since the model proposed by Roussel, is a very commonly used model for cementitious suspensions and because pumping operations of cementitious suspensions or concrete fall within the time window of ca. 60-120 min, the approach by a Roussel model is justified.

In addition, as stated in the assumptions, the effect of a lubrication layer in concrete pumping is not considered, since insights into these effects can be consulted in the literature [21, 28–30]. Hence, the aim of this work is rather to outline the significance and understanding of thixotropy on pumping of concrete or cementitious suspensions only.

For a steady-state solution, thixotropic equilibrium is necessary. Since the flow is one-dimensional in the longitudinal direction, the material derivative simplifies to the partial derivative ($\frac{D\lambda}{Dt} = \frac{\partial\lambda}{\partial t}$). The thixotropic internal structure parameter λ_{eq} should therefore meet conditon (3) to form equilibrium.

$$\lambda_{eq} = \frac{1}{T\alpha\dot{\gamma}} \tag{3}$$

Under temporal equilibrium, Eq. (2) simplifies to Eq. (4a) as a function of the shear rate, which is eventually solved in Eq. (4b).

$$\tau(r) = \tau_0 + \frac{\tau_0}{T\alpha\dot{\gamma}} + \mu\dot{\gamma} \tag{4a}$$

$$\dot{\gamma}^{\pm} = \frac{1}{2\mu}\left[(\tau - \tau_0) \pm \sqrt{(\tau - \tau_0)^2 - 4\frac{\mu\tau_0}{T\alpha}}\right] \tag{4b}$$

Simultaneously this implies that the shear stress τ at a given location as function of pipe radius r should be higher than the total yield stress, including yield stress growth due to thixotropy. In zones where this is not compatible, thixotropic equilibrium cannot be formed and the internal structure continues to grow. In other words, the internal structure parameter diverges in that zone. This zone is not sheared ($\dot{\gamma} = 0$) and is therefore a pure plug zone, as expected for a Bingham fluid [26, 31]. The shear rate would also be zero if the pumping operation would be at rest. With regard to Eq. (3) and Eq. (4a), a zero shear rate does not mean that the internal structure is infinite, it means that the thixotropic structure at rest or in the plug continues to grow to a specific value on a given period of time. On the one hand, during pumping, the total pressure loss is only determined by the rheological properties and the geometry of the sheared zone. Thus, the pressure loss is not dependent on the continuously growing thixotropic structure in the plug. On the other hand, if the pumping operation were at rest it would increase the required pumping pressure after rest. This is a flow-initiation problem as observed in literature [14] and outside the scope of this work.

Hence, temporal equilibrium can only be reached in the sheared zone, where Eq. (4b) has a real valued solution, resulting in conditon (5a). The plug zone is therefore the zone where conditon (5d) is not met.

$$(\tau - \tau_0)^2 \geq 4\frac{\mu\tau_0}{T\alpha} \tag{5a}$$

$$\tau \geq \tau_0\left(1 + \sqrt{\frac{4\mu}{T\alpha\tau_0}}\right) = \tau_0\Lambda \tag{5b}$$

$$\frac{r}{2}\frac{\Delta p}{L} \geq \tau_0\Lambda \tag{5c}$$

$$r \geq \frac{2\tau_0 L}{\Delta p}\Lambda \tag{5d}$$

In other words, the plug radius $R_{p\Lambda}$ is defined by conditon (5d). This expression is reminiscent to the Buckingham-Reiner plug radius $R_{p1} = \frac{2\tau_0 L}{\Delta p}$ amplified by a factor Λ. We refer to this amplification factor as the thixotropy factor. The plug radius for a thixotropic Bingham fluid finally takes the form of Eq. (6), where the actual contribution of thixotropy is referred to as thixotropy addition ζ. It should be noted that these are pure material parameters.

$$R_{p\Lambda} = R_{p1}\Lambda \tag{6}$$

$$\Lambda = 1 + \sqrt{\frac{4\mu}{T\alpha\tau_0}} = 1 + \zeta \tag{7}$$

For non- or insignificant thixotropic Bingham fluids, the characteristic flocculation time T equals infinity or a very high number. This implies that the thixotropy factor Λ equals 1. In other words a pure Bingham plug radius. For common thixotropic fresh concretes, this thixotropy factor lies (but is not restricted to) between 1 and 5. This is based on a range of rheological values common for concrete, as further clarified in 5.1. This means that for the same pressure loss in so-called steady-state situations, the plug radius may mislead observations in case thixotropy is present in a Bingham fluid. The plug radius is namely higher when thixotropy is present.

Lastly, one can rule out one of the two solutions of Eq. (4b). Namely, the second solution (with the minus sign in front of the square root) is considered as non-occurring or the trivial solution. On the one hand, if no significant thixotropy is present ($\Lambda \approx 1$), the shear rate would be equal to zero (*i.e.* trivial solution) and imply slip to allow flow. This is a contradiction with the imposed assumptions. In the case thixotropy is present, it would result in a low, approximately constant value. This implies a very high pressure loss, while the first solution would already have occurred at a smaller value of the pressure loss. This has been explicitly verified and hence only the first solution is meaningful, *i.e.* the one with a plus sign in front of the square root in Eq. (8a). To simplify further use, Eq. (8a) is split into two parts in Eq. (8b), namely part B for Bingham reminiscent part and part T for thixotropy part or the first and second term respectively.

$$\dot{\gamma} = \frac{1}{2\mu}\left[(\tau - \tau_0) + \sqrt{(\tau - \tau_0)^2 - 4\frac{\mu\tau_0}{T\alpha}}\right] \tag{8a}$$

$$= a\left[B\left(r\right) + T\left(r\right)\right] \tag{8b}$$

2.3 Velocity Profile Relation

Making use of a classical expression from fluid mechanics [19, 26, 31], the velocity profile is derived from shear rate Eq. (8a).

$$\dot{\gamma} = \left|\frac{\partial v}{\partial r}\right| = -\frac{\partial v}{\partial r} \tag{9a}$$

$$v\left(r\right) = \int_{r}^{R} \dot{\gamma} dr \tag{9b}$$

After elaboration (Appendix A.1), final Eq. (10) is derived for the velocity profile as a function of radius r, valid for $r \in \left[R_{p\Lambda}, R\right]$. Within the plug radius $r \leq R_{p\Lambda}$, the plug velocity $v_{R_{p\Lambda}}$ can easily be found by evaluating the velocity for the thixotropic plug radius $R_{p\Lambda}$, or as explicitly done in Eq. (A6).

$$\begin{aligned} v\left(r\right) = {} & \frac{1}{2\mu}\left(\left(\frac{\Delta p}{L}\right)\frac{r^2}{4} - \tau_0 r\right)\Bigg|_r^R \\ & + \frac{1}{2\mu}\frac{L}{\Delta p}\left(\left(\frac{\Delta p}{2L}\right)r - \tau_0\right) \\ & \cdot \sqrt{\left(\left(\frac{\Delta p}{2L}\right)r - \tau_0\right)^2 - \sqrt{\frac{4\mu\tau_0}{T\alpha}}^2}\Bigg|_r^R \\ & - \frac{1}{2\mu}\frac{L}{\Delta p} z^2 \ln\Bigg\{\left(\left(\frac{\Delta p}{2L}\right)r - \tau_0\right) \\ & + \sqrt{\left(\left(\frac{\Delta p}{2L}\right)r - \tau_0\right)^2 - \sqrt{\frac{4\mu\tau_0}{T\alpha}}^2}\Bigg\}\Bigg|_r^R \end{aligned} \tag{10}$$

To facilitate further use, the velocity profile is expressed as a function of symbolic, but meaningful, parameters or functions (b, δ, z, e and s) through Eq. (11).

$$v\left(r\right) = a\left(b\frac{r^2}{2} - \delta r\right)\Bigg|_r^R + \frac{a}{2b} es\Big|_r^R - \frac{a}{b}\frac{z^2}{2}\ln\left(e+s\right)\Bigg|_r^R \tag{11}$$

with :

δ	:	τ_0
a	:	$\frac{1}{2\mu}$
b	:	$\left(\frac{\Delta p}{L}\right)\frac{1}{2}$
e	:	$br - \delta$
s	:	$\sqrt{e^2 - z^2}$
z	:	$\sqrt{\frac{4\mu\tau_0}{T\alpha}}$

2.4 Discharge Relation

Lastly, the pressure loss - discharge relationship can be derived by integrating the entire velocity profile over the pipe cross-section (*i.e.* flux integration). This yields the following expressions.

$$Q = \int_0^R \int_0^{2\pi} v\left(r\right) d\theta r dr \tag{12a}$$

$$= \pi R_{p\Lambda}^2 v_{R_{p\Lambda}} + 2\pi \int_{R_{p\Lambda}}^{R} r v\left(r\right) dr \tag{12b}$$

Substituting Eq. (11) in Eq. (12b), one obtains the following expression, bearing in mind that $r = \frac{1}{b}\left(e + \delta\right)$ and $dr = \frac{de}{b}$.

$$\begin{aligned} Q = {} & \pi R_{p\Lambda}^2 v_{R_{p\Lambda}} + 2\pi a \int_{R_{p\Lambda}}^{R}\left(b\frac{r^2}{2} - \delta r\right)\Bigg|_r^R r dr \\ & + 2\pi\frac{a}{2b^3}\int_{R_{p\Lambda}}^{R}\left(e+\delta\right) es\Big|_r^R de \\ & - 2\pi\frac{az^2}{2b^3}\int_{R_{p\Lambda}}^{R}\left(e+\delta\right)\ln\left(e+s\right)\Big|_r^R de \end{aligned} \tag{13}$$

Further elaboration is required to easily resolve Eq. (13). Therefore, the discharge rate Q is firstly decomposed into a plug part Q_p and a sheared part Q_s (Eq. (14)). After that, a decomposition of Q_s, is made into a Bingham part Q_{sB} and a thixotropy part Q_{sT}. The thixotropy part Q_{sT} is then further unravelled (Eq. (15)) to facilitate the final solution.

$$Q = Q_p + Q_{sB} + Q_{sT} \tag{14}$$

$$Q_{sT} = \sum_{j=1}^{4} Q_{sTj} \tag{15}$$

The solution of all decomposed parts can be found in Appendix A.2, through Eq. (A14) to Eq. (A16d). To evaluate these explicit functions, it is useful to substitute the following a priori known values:

$$\Lambda = \left(1 + 2\sqrt{\frac{\mu}{T\alpha\tau_0}}\right) = 1 + \zeta \tag{16a}$$

$$R_{p\Lambda} = R_{p1\Lambda} = \frac{2\tau_0 L}{\Delta p}\Lambda \tag{16b}$$

$$e\big|^{R_{p\Lambda}} = z \tag{16c}$$

$$s\big|^{R_{p\Lambda}} = \sqrt{e^2 - z^2}\Big|^{R_{p\Lambda}} = 0 \tag{16d}$$

More insights and more elegant expressions can still be found via a dimensionless transformation.

3 Dimensionless Formulation

To gain insights and elegance, the shear rate profile, velocity profile and discharge relation are reformulated as functions of dimensionless parameters. Such a transformation reveals important dimensionless parameters, as well as their proportionality to the considered quantity. From now on, the latter relations are therefore rewritten as functions of dimensionless parameters and a respective units proportionality is written between brackets. Since the shear rate, velocity and discharge have a dimension unit, a units proportionality appears as a consequence.

The dimensionless transformation starts from the most important dimensionless number, *i.e.* the Bingham number Bn. To facilitate the interpretation, the inverse Bingham number is used since in practice the applied pumping pressure is typically related to the discharge rate by a pressure loss-discharge curve. It is also scaled by a factor of 2, so that a dimensionless pipe wall shear stress $\widehat{\tau}_w$ is obtained instead, because then it is more intuitive to relate the pumping operation to flow initiation. Flow initiates when the pipe wall shear stress τ_w overcomes the yield stress τ_0. Hence, one obtains the dimensionless wall shear stress number in Eq. (17), and since it is directly related to the pumping pressure Δp, we refer to it as the pumping pressure number Pn.

$$Pn = \frac{1}{2Bn} = \widehat{\tau}_w = \frac{\tau_w}{\tau_0} = \frac{\Delta p R}{2L\tau_0} \tag{17}$$

The dimensions from important parameter z and functions e and s are then decoupled as follows:

$$z = \delta\zeta \qquad \zeta = \Lambda - 1 \tag{18}$$

$$e = \delta\varepsilon \qquad \varepsilon = Pn\left(\frac{r}{R}\right) - 1 \tag{19}$$

$$s = \delta\sigma \qquad \sigma = \sqrt{\varepsilon^2 - \zeta^2} \tag{20}$$

The radial coordinate r is transformed to r/R and the plug radii are also transformed:

$$R_{p1} = \frac{R}{Pn} \qquad R_{p\Lambda} = \frac{R}{Pn}(1 + \zeta) \tag{21}$$

with :

Pn	:	Pressure number
b	:	Scaled pressure loss
δ	:	Yield stress τ_0
Λ	:	Thixotropy factor
ζ	:	Dimensionless thixotropy addition
ε	:	Dimensionless corrected shear stress
σ	:	Dimensionless thixotropically corrected shear stress
z	:	Thixotropy addition
e	:	Corrected shear stress
s	:	Thixotropically corrected shear stress
R_{p1}	:	Bingham plug radius
$R_{p\Lambda}$	:	Thixotropic plug radius

Hence, to facilitate interpretations and overall expressions in this work, the pressure number Pn is used instead of the Bingham number Bn even though they represent the same physical matter. In that way, pipe flow initiates for $Pn \geq 1$ (or $Bn \leq 0.5$). In literature, the Bingham number Bn may be defined slightly differently, as long as it is the proportion of a yield stress contribution to a (viscous) stress contribution [10, 17, 18].

3.1 Dimensionless Transformation

Making use of Eq. (17) to Eq. (21), all expressions are transformed into dimensionless ones. All dimensionless parameters are written by a hat $\widehat{\cdot}$ or as Greek characters, except for rheological parameters μ, $\tau_0 = \delta$, τ, $\dot{\gamma}$ and dimensionless numbers *e.g.* Pn, Bn etc.

3.1.1 Dimensionless Shear Rate Formulation

One can rewrite Eq. (22a), by making use of the pressure number $Pn = \frac{\tau_w}{\tau_0} = \frac{\Delta p R}{2L\tau_0}$. The term between brackets defines the dimension of the relation, since all other terms are dimensionless. Hence it forms an important dimension scale or proportionality for the considered relation.

$$\dot{\gamma} = \frac{1}{2}\left[\frac{\tau_0}{\mu}\right]\left(Pn\frac{r}{R} - 1\right)\left(1 + \sqrt{1 - \left(\frac{\Lambda - 1}{Pn\frac{r}{R} - 1}\right)^2}\right) \tag{22a}$$

$$\dot{\gamma} = \frac{1}{2}\left[\frac{\tau_0}{\mu}\right]\left(\varepsilon|^r + \sigma|^r\right) \tag{22b}$$

As a result, elegant dimensionless formulation (22b) for the shear rate is found. Moreover, an important inverse time scale or shear rate proportionality is revealed as well: $\left[\tau_0/\mu\right]$. In fluid mechanics this is usually referred to as the

advective time scale, although it is usually defined for non-yield stress fluids by the viscosity and a velocity proportionality [32]. In conclusion, the shear rate is proportional to this inverse time scale and as such, so are the velocity and discharge as well.

3.1.2 Dimensionless Velocity Profile Formulation

The same approach is followed to transform the velocity profile into Eq. (23), valid for $r \in [R_{p\Lambda}; R]$. In dimensionless form the significance of terms and proportionalities can be observed again.

$$v(r) = \frac{1}{2}\left[\frac{\tau_0 R}{\mu}\right]\left\{\left(\frac{r}{R}\right)\left(\frac{Pn}{2}\left(\frac{r}{R}\right)-1\right)\Big|_r^R + \frac{1}{2Pn}\left(\varepsilon\sigma|_r^R - \zeta^2 \ln\left(\delta\left(\varepsilon+\sigma\right)\right)\Big|_r^R\right)\right\} \tag{23}$$

Similar to the shear rate, a velocity proportionality is revealed: $\left[\tau_0 R/\mu\right]$. This proportionality is the inverse time scale, scaled by the pipe radius R. In dimensionless form, the plug velocity simplifies to the following expression:

$$v_{R_{p\Lambda}} = \frac{1}{2}\left[\frac{\tau_0 R}{\mu}\right]\left\{\left(\frac{Pn}{2}-1\right) - \frac{\zeta^2-1}{2Pn} + \frac{1}{2Pn}\left(\varepsilon\sigma|^R - \zeta^2 \ln\left(\frac{\varepsilon+\sigma}{\zeta}\right)\Big|^R\right)\right\} \tag{24}$$

3.1.3 Dimensionless Discharge Formulation

Lastly, one can do the same for the discharge relation to reveal important dimensionless parameters and dimension proportionalities. After elaboration of the decomposed discharge parts (Appendix A.3), one finally obtains Eq. (25).

$$Q = \frac{\pi}{48}\left[\frac{\tau_0 R^3}{\mu}\right]\frac{1}{Pn^3}\cdot \begin{pmatrix} 6Pn^4 - 8Pn^3 + 2\left(1+\zeta\right)^3\left(1-3\zeta\right) \\ + 6\,\varepsilon^3\sigma\Big|^R + 24\,\varepsilon^2\sigma\Big|^R + 3\,\varepsilon\sigma|^R\left(4-\zeta^2\right) \\ - 24\zeta^2\,\sigma|^R - 8\,\sigma^3\Big|^R \\ - 3\zeta^2\left(4+\zeta^2\right)\ln\left(\frac{\varepsilon+\sigma}{\zeta}\right)\Big|^R \end{pmatrix} \tag{25}$$

For the discharge relation, the same inverse time scale appears, scaled by the pipe radius to the power of three: $\left[\tau_0 R^3/\mu\right]$. Likewise, also the flow rate Q is proportional to the this discharge scale. The discharge proportionality is the same as proposed by Billingham and Ferguson [17] to facilitate dimensionless expressions: $\widehat{Q} = Q/(\tau_0 R^3/\mu)$.

3.2 Alternative Interpretation

Dimensionless formulas usually outline important dimensionless numbers, in this case for thixotropic pipe flow. One can namely interpret ε as a dimensionless corrected shear stress, because it is in fact the dimensionless form of the radial shear stress τ subtracted by the yield stress τ_0. The thixotropy addition ζ represents the predominance of the Bingham time scale μ/τ_0 versus the thixotropy time scale $T\alpha$, which is reminiscent to the Deborah number (*i.e.* a thixotropic time scale versus an advective time scale [17]). Alternatively, one could see ζ as the ratio of the thixotropic shear scale to the Bingham shear scale τ_0/μ.

Similar to ε, σ is the shear stress corrected for thixotropy. In fact it is the dimensionless thixotropic projection of the corrected shear stress. Looking closely to this analogy, one can express ε, ζ or σ as a function of one another. Thus, they imply a triangular relationship: $\varepsilon^2 = \sigma^2 + \zeta^2$, enclosing an angle called ϕ defined in Eq. (26) (Figure 2). This angle is called the thixotropy angle ϕ, because it determines the degree of thixotropy of the considered pipe flow conditions. It is a measure for the predominance of thixotropic flow behaviour versus time-independent flow behaviour. This concept also applies to dimensioned forms as functions of e, z and s. Thixotropy angle ϕ is defined by this triangle concept (Figure 2):

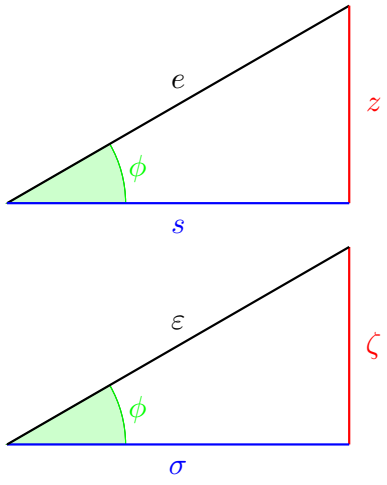

Figure 2: Dimensionless variables (top) e, z and s or (bottom) ε, ζ and σ form a rectangular triangle enclosing angle ϕ. The thixotropy angle ϕ is a degree for the significance of a thixotropic flow regime versus a time-independent flow regime.

$$\sin(\phi) = \frac{\zeta}{\varepsilon} = \frac{\Lambda - 1}{Pn\left(\frac{r}{R}\right) - 1} \tag{26}$$

A thixotropy angle close to 0 implies that thixotropy effects are negligible in respective flow conditions, while a

thixotropy angle of $\frac{\pi}{2}$ (90°) is the most significant. Since ε and σ have a radial profile, also the thixotropy angle ϕ has a radial profile. At a considered radial distance r in the pipe, thixotropy angle ϕ_r thus literally represents the degree of thixotropy significance. Where 0 means insignificant, while $\frac{\pi}{2}$ (90°) means predominant.

The overall influence of thixotropy on the considered flow conditions can be assessed by the angle of thixotropy ϕ_R at the pipe wall ($r = R$), just as the overall pressure loss in a pipe is determined by the shear stress τ_w at the pipe wall, and thus represented by the pressure number Pn. In the case that there is no influence of thixotropy, the thixotropy angle ϕ would be 0. Then, Eq. (26) implies that the material is either non-thixotropic ($\Lambda = 1$), which is the trivial solution, or either that the thixotropic behaviour has been completely overcome ($Pn = \infty$). This would mean that the pressure loss is extremely high and thus also the corresponding discharge. Thereby no significant thixotropy effects are observed ($\phi \approx 0$).

If the influence of thixotropy were at maximum, the thixotropy angle ϕ would be $\frac{\pi}{2}$ (90°). This would imply that the pressure number Pn equals the thixotropy factor Λ ($Pn = \Lambda$). In other words, to initiate thixotropic flow, one should overcome the thixotropic initiation pressure $\Delta p_{i\Lambda}$, which is the Bingham initiation pressure amplified by the thixotropy factor Λ as in Eq. (27).

$$\Delta p_{i\Lambda} = \Lambda \frac{2L\tau_0}{R} = \Lambda \Delta p_{i\Lambda=1} \tag{27}$$

In all other cases, there still is an influence of thixotropy, but somewhere between a completely thixotropic flow regime or none at all.

3.3 Alternative Dimensionless Formulations

Since ε, ζ and σ are triangularly related to one another by thixotropy angle ϕ and ε is related to the pressure number Pn, one can rewrite the discharge relation as a function of either the pressure number Pn and thixotropy angle ϕ, or either ε and thixotropy angle ϕ. In addition, an analogy (28) in mathematical shape exists between Pn and Λ versus ε and ζ:

$$\begin{pmatrix} \varepsilon|^R \\ \zeta \end{pmatrix} = \begin{pmatrix} Pn - 1 \\ \Lambda - 1 \end{pmatrix} \tag{28}$$

Several alternative formulations can be found facilitating elegance and thus the ease of calculation or implementation in software. These alternative formulations can be consulted in Appendix C.

4 Verification

Even though all derived equations have been verified step-by-step via mathematical software Maple®, yet another verification is made when the model is applied to a non-thixotropic Bingham fluid. Without thixotropy the solution should simplify to the solution for a Bingham model, which is called the Buckingham-Reiner equation [33].

4.1 Buckingham-Reiner

For a Bingham model, the analytical solution for Poiseuille flow was originally developed by Buckingham and Reiner [22, 26, 31, 33]. Hence the pressure loss discharge relation was named after both, namely the Buckingham-Reiner equation. For ease of comparison, the Buckingham-Reiner and related equations are rewritten in their dimensionless form, making use of the pressure number Pn. It is remarkable that the same dimension proportionalities between brackets are also valid for the Bingham model.

$$\dot{\gamma}(r) = \left[\frac{\tau_0}{\mu}\right]\left(Pn\left(\frac{r}{R}\right) - 1\right) \tag{29}$$

$$v(r) = \left[\frac{\tau_0 R}{\mu}\right]\left(\frac{Pn}{2}\left(1 - \left(\frac{r}{R}\right)^2\right) + \left(\frac{r}{R}\right) - 1\right) \tag{30}$$

$$Q = \frac{\pi}{12}\left[\frac{\tau_0 R^3}{\mu}\right]\left(3Pn - 4 + Pn^{-3}\right) \tag{31}$$

4.2 Bingham Model Comparison

No thixotropy means that the characteristic flocculation time T is equal to infinity and further simplifies the following set A of dependent parameters or function simplifications:

$$A = \begin{pmatrix} T = +\infty & \Lambda = 1 \\ z = 0 & \zeta = 0 \\ s = e & \sigma = \varepsilon \end{pmatrix} \tag{32}$$

Substituting non-thixotropic set of parameters A (in limit) in the respective shear rate Eq. (22b), the velocity profile Eq. (23) and the discharge Eq. (25) yield the following formulas, after substitution of the dimensionless corrected shear stress $\varepsilon = Pn\left(\frac{r}{R}\right) - 1$ and further simplification:

$$\begin{aligned} \dot{\gamma}(r) &= \frac{1}{2}\left[\frac{\tau_0}{\mu}\right]\left(2\varepsilon|^r\right) \\ &= \left[\frac{\tau_0}{\mu}\right]\left(Pn\left(\frac{r}{R}\right) - 1\right) \end{aligned} \tag{33}$$

$$v(r) = \frac{1}{2}\left[\frac{\tau_0 R}{\mu}\right]\left\{\left(\frac{r}{R}\right)\left(\frac{Pn}{2}\left(\frac{r}{R}\right)-1\right)\Big|_r^R + \frac{\varepsilon^2\big|_r^R}{2Pn}\right\} \quad (34)$$

$$= \left[\frac{\tau_0 R}{\mu}\right]\left(\frac{Pn}{2}\left(1-\left(\frac{r}{R}\right)^2\right)+\left(\frac{r}{R}\right)-1\right)$$

$$Q = \frac{\pi}{48}\left[\frac{\tau_0 R^3}{\mu}\right]\frac{1}{Pn^3} \quad (35)$$

$$\cdot\begin{pmatrix} 6Pn^4 - 8Pn^3 + 2 \\ +\,6\,\varepsilon^4\big|^R + 24\,\varepsilon^3\big|^R + 12\,\varepsilon^2\big|^R \\ -\,8\,\varepsilon^3\big|^R \end{pmatrix}$$

$$= \frac{\pi}{12}\left[\frac{\tau_0 R^3}{\mu}\right]\left(3Pn - 4 + Pn^{-3}\right)$$

Eventually, the equations become equivalent to the Buckingham-Reiner equations, quod erat demonstrandum.

5 Results and Significance

This section is dedicated to the results and significance of thixotropy. Since we aim to apply it for a concrete pumping application, the model is applied to fresh concrete rheology in some practical calculation examples. A comparison is made with the developed model and other rheological models commonly applicable to fresh concrete.

First, rheological values and pipe geometries common for concrete pumping are outlined. Then, the shear profiles are compared with the delivered model in this work and other applicable models. Lastly, this is also done for the velocity profile and discharge diagram (*i.e.* diagram of discharge relation).

5.1 Concrete Pumping

The range of the considered rheological parameters is outlined first, before the actual model comparisons are made. A practical set of rheological parameters is based on common values used for fresh concrete pumping. DN100 and DN125 are commonly used pipe diameters for concrete pumping. Therefore, a DN100 (*e.g.* with inner radius $R = 52.65\ mm$) is considered in the calculation examples. Based on Feys [34], the discharge for concrete pumping for these pipe diameters generally varies between 2.5 to 10 L/s, which is used in the calculation examples.

Fresh concrete rheology often considers a Bingham model or a modified Bingham model, as defined in Eq. (36) and Eq. (37) respectively [26, 31]. The Bingham model includes a yield stress τ_0, which should be overcome to initiate flow, after which the flow resistance is defined by the plastic viscosity μ. The modified Bingham model has a shear thickening or thinning effect c in addition [31].

$$\tau = \tau_0 + \mu\dot{\gamma} \quad (36)$$

$$\tau = \tau_0 + \mu\dot{\gamma} + c\dot{\gamma}^2 \quad (37)$$

Although these two models do not take into account time-dependent effects, they are often considered as appropriate for fresh concrete rheology. Analytical solutions for pipe flow exist for these two models (Appendix D). The Poiseuille flow extension for the modified Bingham model can also be formulated as a function of dimensionless parameters and function variables. An additional parameter is, however, necessary to describe shear thickening/ thinning, namely the modified Bingham number $MBn = \frac{4c\tau_0}{\mu^2}$. This represents the ratio of the shear thickening time scale c/μ to the Bingham time scale μ/τ_0.

In addition, a wide application range of rheological parameters exists, as provided in rheograms for fresh concrete [35]. A single set (Table 1) of rheological parameters representative for fresh concrete (self-compacting concrete) is used, based on literature [31, 35].

Table 1: The rheological values used for comparison are representative for fresh concrete [31, 35].

Rheological Model	$\tau_0\ [Pa]$	$\mu\ [Pa.s]$	$c\ [Pa.s^2]$
Bingham	100	10	
Modified Bingham	100	10	0.2

Thixotropy can be significant in self-compacting concrete. The deflocculation rate α is usually approximated as 0.005 for concrete [2], while the characteristic flocculation time T varies. Strongly thixotropic concretes correspond to a T-value of 200 s or less [2]. The range of plastic viscosity ($\approx$ 10-100 $Pa.s$) and yield stress ($\approx$ 25-100 Pa) implies that the thixotropy factor Λ lies between approximately 1 and 5 for thixotropic fresh concretes (but not restricted to). Therefore a thixotropy range of 1-5 is used to distinguish the significance of thixotropy on the flow regime during pumping of such self-compacting concretes.

Once the rheological parameters for a common self-compacting concrete are outlined, the shear rate profile, velocity profile and discharge profile can be compared for different applicable models.

5.2 Shear Rate Profiles

Since concrete is a yield stress fluid, plug flow occurs in the pipe during pumping. This plug is defined by its plug radius (Eq. (21)) and is non-sheared. One clearly observes in Figure 3 that a thixotropy factor Λ equal to 1 coincides with the shear profile of a pure Bingham fluid. Figure 3 shows that a constant flow rate of $2.5\ L/s$ ($\widehat{Q} = 0.55$) results in an increasing plug radius for an increasing thixotropy factor Λ.

However, Eq. (21) should not be misinterpreted that the plug radius is amplified by the thixotropy factor Λ for a constant flow rate Q. Instead, the plug radius is only amplified by the thixotropy factor Λ if the pressure number Pn remains constant. For a constant discharge Q, with a different thixotropy, the pressure number Pn is different. In other words, for a constant flow rate, the pumping pressure, pressure loss or pressure number is higher for higher thixotropy levels.

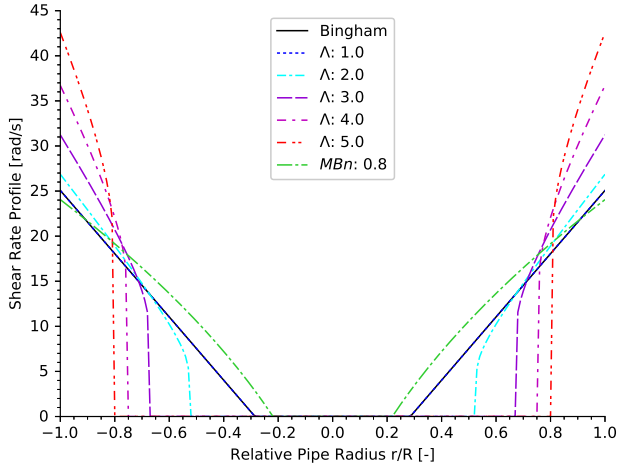

Figure 3: The shear rate profiles for a constant discharge Q of $2.5\ L/s$ ($\widehat{Q} = 0.55$ with $R = 52.65\ mm$) shows that thixotropy causes the shear to be non-linear and has a significant increasing effect on the plug zone, which is the region where the shear rate is zero.

In addition, higher pressure numbers result in smaller plug radii (Eq. (21)), however amplified by the thixotropy factor Λ, such that the effective plug radius is still significantly higher than for a Bingham fluid with the same discharge. This causes the shear rates near the pipe wall to be significantly higher than for a Bingham fluid or modified Bingham fluid.

Unlike a Bingham fluid, the shear rate profile is non-linear for a thixotropic fluid. This is also the case for a modified Bingham type of fluid. For the latter types, the plug radius is insignificantly smaller than for a Bingham fluid.

An increase in flow rate to $10\ L/s$ ($\widehat{Q} = 2.18$) causes the plug to decrease for a thixotropic fluid (Figure 4). This is logical because a higher flow rate results in higher shear rates and thus more thixotropic structure that is broken down in equilibrium. In fact, a balance exists between shear action and thixotropic build-up. This balance clearly shifts by an increasing plug radius for higher thixotropy factors Λ.

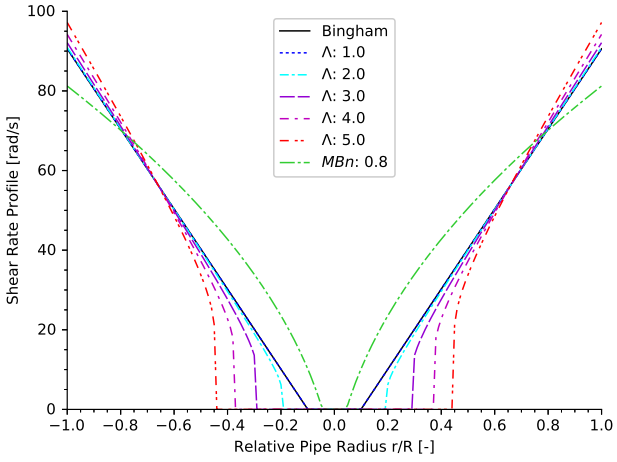

Figure 4: An increased flow rate Q of $10\ L/s$ ($\widehat{Q} = 2.18$ with $R = 52.65\ mm$) reveals a shifting equilibrium between shear action and thixotropic structure build-up. Again, the plug zone (region where $\dot{\gamma} = 0$) also increases with an increasing thixotropy factor Λ.

These results clearly show that a different flow regime is going on for a thixotropic fluid compared to a Bingham and modified Bingham fluid. The shear rate profile is a first fundamental view on the difference between flow for a thixotropic fluid and other non-thixotropic fluids. The shear rate profile can, however, not directly be measured in case of pipe flow geometries. One can instead indirectly measure the shear rate profile by a measurement of the velocity profile, despite experimental noise. Some equipment exists to measure the velocity profiles in pipe flow geometries, such as particle image velocimetry, magnetic resonance or ultrasonic velocity profiling techniques [36–41].

Therefore, the analysis of the velocity profiles for thixotropic fluids compared to non-thixotropic fluid gives a second image of the significance of thixotropic effects.

5.3 Velocity Profiles

The velocity profile is a second measure on the significance of thixotropy in pipe flow (Poiseuille flow). It is indirectly related to the shear rate and vice versa. Therefore the velocity profile is analysed for thixotropic flow in this section.

As expected, the velocity profile (Figure 5) with a thixotropy factor Λ of 1 also coincides with the velocity profile for a Bingham fluid. For increasing thixotropy values Λ, the plug increases as elaborated for the shear rate profile (section 5.2).

For a Bingham and modified Bingham fluid the velocity profile is smooth, which means that its derivative (the shear rate profile) is continuous. This is remarkably not the case for a thixotropic velocity profile. In other words, there is a jump in the shear rate profile for a thixotropic material (Figure 3). This gap in shear rate profile or non-smoothness in the velocity profile is the transition point from the plug to the shear zone. Due to thixotropic structural build-up, a non-equilibrium exists in the plug, where the thixotropic internal structure continues to grow. This causes a clear gap in shear rate, or non-smoothness in the velocity profile.

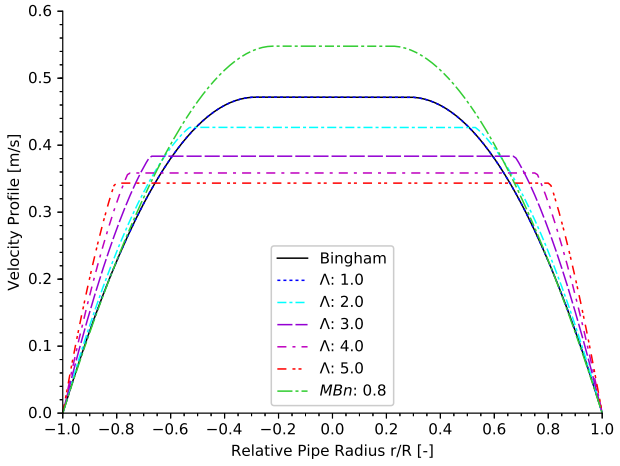

Figure 5: The velocity profile for various thixotropy factors Λ show that thixotropy can have a significant effect on a smooth transition from plug flow to shear flow. Higher thixotropy levels cause higher plug radii and in return lower plug velocities, however higher shear rates or velocity development near the pipe wall. ($\widehat{Q} = 0.55$ with $R = 52.65\ mm$)

On the one hand, the plug velocity is smaller due to a wider plug to compensate for the conservation of mass for a constant discharge Q. On the other, the velocity near the outer boundary has to be higher (Figure 5). This means that more velocity needs to be developed over a smaller outer zone, thus resulting in higher shear rates and higher required pumping pressures.

An increased flow rate of 10 L/s ($\widehat{Q} = 2.18$) leads to smaller plug radii, increasing for thixotropy factors Λ. However, more important to notice is that the velocity profile tends more to the Bingham velocity profile for a higher discharge rate (Figure 6). This is because the balance of shear action versus thixotropic build-up gains more weight for the shear action.

One could wonder if for very high flow rates Q, thixotropy becomes less important and pipe flow can be approximated by the Buckingham-Reiner equations. In fact this is the case, the thixotropic flow eventually asymptotically approximates the Buckingham-Reiner solution for higher flow rates. This is shown in this work by the comparison of the discharge diagrams for thixotropic fluids versus non-thixotropic fluids.

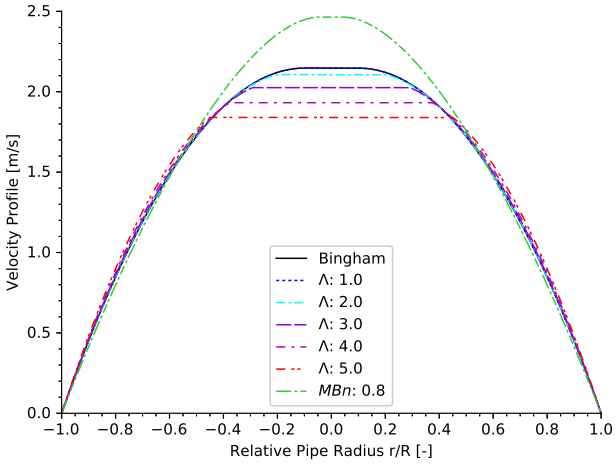

Figure 6: For a higher discharge rate of 10 L/s ($\widehat{Q} = 2.18$ with $R = 52.65\ mm$), the velocity profile shows to have a smaller plug, yet bigger plug for increasing thixotropy factors Λ. The transition from plug to shearing happens more smooth for a higher flow rate, because the flow regime approximates a Bingham flow more.

5.4 Discharge Diagram

In the design of pumps, typically the working discharge is plotted versus the pressure output. Therefore, also the discharge Q is plotted versus the pressure loss $\Delta p/L$ in this section. Not only because this diagram relates to the practical choice of a pump, but also because it is the direct output of pumps in practice. Moreover, the pres-

sure loss/discharge diagram is modified to a dimensionless form. This is a powerful way to express the pressure loss in general, but also to point out the significance of thixotropic pipe flow compared to non-thixotropic fluids.

For comparison of the discharge, a diagram is therefore made where the pressure number Pn is plotted as a function of the dimensionless discharge $\widehat{Q}$. This is the discharge divided by its respective dimension proportionality, as done by Billingham and Ferguson [17]. Similarly one can define the dimensionless velocity $\widehat{v}$ as well as shear rate $\widehat{\dot{\gamma}}$ and shear stress $\widehat{\tau}$ through Eq. (38).

$$\widehat{Q} = \frac{Q}{\frac{R^3\tau_0}{\mu}} \quad \widehat{v} = \frac{v}{\frac{R\tau_0}{\mu}} \quad \widehat{\dot{\gamma}} = \frac{\dot{\gamma}}{\frac{\tau_0}{\mu}} \quad \widehat{\tau} = \frac{\tau}{\tau_0} = Pn\left(\frac{r}{R}\right) \tag{38}$$

The discharge profile for every Bingham fluid is therefore exactly the same. A single curve in the diagram (Figure 7) maps the flow behaviour of every possible combination of Bingham rheological parameters. This is why the dimensionless discharge number $\widehat{Q}$ is more important to describe laminar pumping behaviour for yield stress fluids, than for instance the Reynolds number Re which is usually used to describe turbulent flow behaviour [19]. This, moreover, makes the discharge diagram a powerful way to distinguish effects of other rheological models such as the thixotropy model developed in this work, but also the modified Bingham model. For potential future use, the numerical values corresponding to the discharge diagrams are also depicted in tables in Appendix E. The pressure loss number Pn, thixotropy angle ϕ_R, dimensionless plug velocity $\widehat{v}_{R_{p\Lambda}}$ and the dimensionless wall shear rate $\widehat{\dot{\gamma}}_R$ are depicted as a function of the dimensionless discharge $\widehat{Q}$.

One clearly observes that the pumping behaviour of a Bingham fluid is linear for the larger part of flow rates. It becomes non-linear for lower flow rates or lower pressure numbers $\approx Pn < 1.5$ (Figure 8). In the regime where the pressure number Pn is lower than approximately 1.5, the lower order (Pn^{-3}) term in the Buckingham-Reiner Eq. (31) plays a significant role, while it is otherwise negligible for the overall pumping behaviour.

For a zero discharge, the pressure number Pn equals the thixotropy factor Λ ($Q = 0$ for $Pn = \Lambda$ in Eq. (C2), see Figure 8). This is an important aspect for flow initiation pumping pressure. The initiation pressure should be Λ times higher than the initiation pressure for a Bingham or modified Bingham fluid. Moreover, this is also an important property because it can be used to determine the thixotropy factor experimentally after transformation of the pressure loss - discharge diagram.

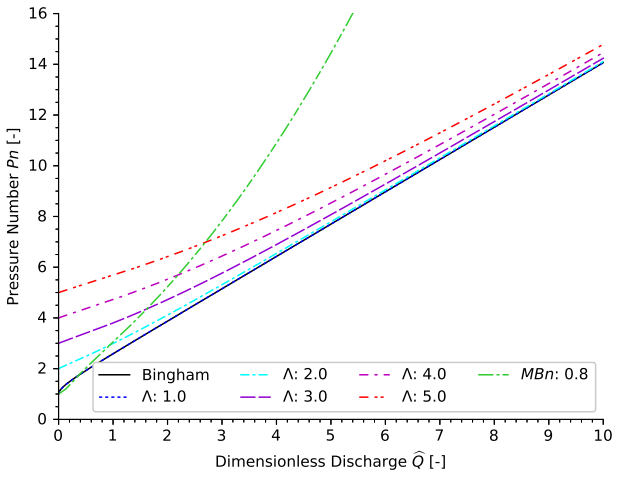

Figure 7: The discharge diagram is a powerful tool to distinguish thixotropy in the pumping behaviour. Every combination of the Bingham model is represented by a single profile. The higher the thixotropy factor Λ, the higher the influence of thixotropy on the flow regime. The thixotropy effect asymptotically wears down to the Bingham profile for larger flow rates $\widehat{Q}$.

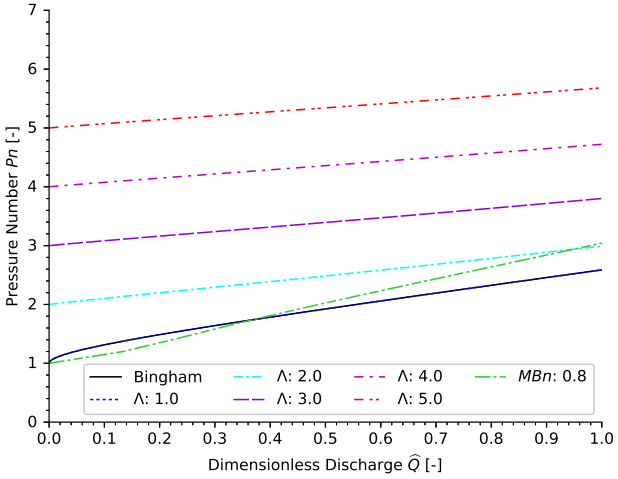

Figure 8: The discharge diagram becomes non-linear for a Bingham fluid for pressure numbers smaller than ca. 1.5, where lower order terms in the Buckingham-Reiner equation are no longer negligible. For a thixotropy fluid, the initiation pumping pressure, where the discharge is theoretically zero, is equivalent with the Bingham initiation pressure amplified by thixotropy factor Λ.

5.4.1 Pumpbability Contribution

Another remarkable aspect of the dimensionless discharge diagram for the Bingham and modified Bingham model, is the point where the pressure number Pn equals 2. Then,

the yield stress τ_0 contributes as much as the plastic viscosity μ to the pumping pressure (loss).

A similar point could be defined in the thixotropic discharge diagram, namely the point where $Pn = 2\Lambda$. This means that the contribution of the thixotropically increasing yield stress is equal to the contribution of plastic viscous energy dissipation. This point could be an important point to design the pumpability of the considered fluid.

On the one hand, if the rheological properties are fixed for the industrialised process, one could change the discharge rate or pipe geometry so a more desirable pumping pressure could be achieved or vice versa. On the other hand, when the flow rate or geometry cannot be changed in an industrial pumping operation, one can achieve a more desirable pumping pressure (required pumping power) by changing the rheological properties. Hence, it is called the pumpability contribution point and defined by Eq. (39).

$$\widehat{Q}_c = \widehat{Q}\,(Pn = 2\Lambda) \tag{39}$$

This may be used as a design point, relating the discharge, geometry, pressure loss and rheological properties. Calculation examples for thixotropy factors between 1 and 5, applicable for fresh concrete, are depicted in Table 2.

Table 2: The dimensionless discharge $\widehat{Q}_c$ calculated for the point where the pumpablity contribution is the same for the plastic viscosity as for the thixotropically grown yield stress. This interpretation may be useful as a design point for the pumping application.

Λ	1	1.5	2	3	4	5
$\widehat{Q}_c$	0.56	2.30	4.00	7.39	10.78	14.16

That is why for self-compacting concrete compared to traditional concrete a wider pipe diameter is usually chosen. Since self-compacting concrete has a higher plastic viscosity, one can decrease the pumping pressure contribution by the plastic viscosity μ, while sustaining a high discharge rate Q with reasonable required pumping power [22, 31, 34, 42].

5.4.2 Buckingham-Reiner Asymptote

Lastly, one more diagram is made which expresses the relative difference of a thixotropic fluid versus a Bingham fluid, defined by Eq. (40). The pressure number Pn_Λ for a thixotropic fluid is reduced by the reference for a Bingham fluid ($Pn_{ref} = Pn_1$) and divided by this reference. This transformation is obtained by numerically inverting Eq. (25).

$$\frac{\Delta Pn}{Pn_{ref}}(q) = \frac{Pn_\Lambda(q) - Pn_1(q)}{Pn_1(q)} \tag{40}$$

This results in Figure 9, expressing how much the predicted pumping pressures can be off for various thixotropic fluids, compared to their Bingham equivalents. For low discharges, the contribution of thixotropy can be very underestimated, more specifically by a fraction of $\Lambda - 1 = \zeta$ for a zero discharge. Hence ζ is called the thixotropy addition. For higher discharges, the significance exponentially fades until the Bingham solution is asymptotically approached (*i.e.* Buckingham-Reiner equation). The lower the thixotropy value Λ, the faster the Bingham solution is approached. Therefore, one could define a certain threshold for which the thixotropic flow regime could be approximated by the Bingham solution, *e.g.* a relative difference smaller than 5%.

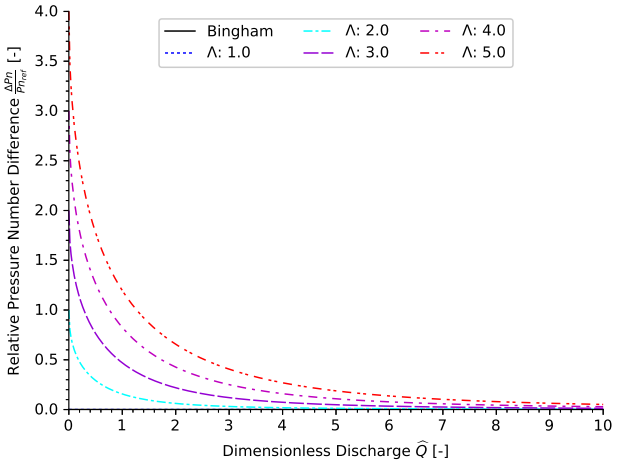

Figure 9: The pressure number Pn is numerically inverted from Eq. (25) and the relative difference with the Bingham-Reiner equation (Pn_{ref}) is plotted as a function of dimensionless discharge $\widehat{Q}$. This shows how much more pumping pressure is relatively required for a thixotropic fluid compared to a non-thixotropic Bingham fluid.

By the alternative interpretation of the developed model, one knows that the thixotropy angle ϕ_R is the actual degree of thixotropic flow regime. Hence great similarity can be found between the significance in Figure 9 and the thixotropy angle ϕ_R in Figure 10. Alternatively, one could also define a certain threshold for the thixotropy angle ϕ_R (*e.g.* 5°) for which thixotropic pumping could be approximated by the Buckingham-Reiner equation.

Conceptually, one could further extend the interpretation of the thixotropy influence on the pumping behaviour

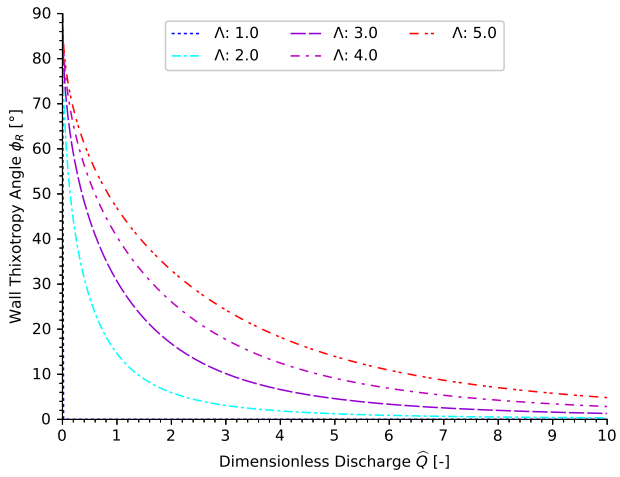

Figure 10: By an alternative interpretation through the thixotropy angle ϕ_R it can also be observed that the influence of thixotropy fades exponentially for higher discharges and lower thixotropy factors Λ.

for different rheological base models (*e.g.* modified Bingham, Herschel-Bulkley etc.). For a thixotropic modified Bingham model for instance, thixotropy would have a similar relative addition as in Figure 9 for the modified Bingham model. Although this is theoretically not fully accurate, it forms an intuitive interpretation of the thixotropy influence on the pumping flow regime.

6 Summary and Discussion

In this work we derived a new extension to Poiseuille flow applicable to thixotropic concretes and cementitious suspensions. The extension is derived for a model proposed by Roussel [2], which is commonly used to model thixotropy in fresh concrete and cementitious suspensions. This model is a general model that can be applied to fresh concrete rheology, but is not limited to it. For thixotropy also other more complicated models exist, however, the derived model in this work yet remains elegant and provides deeper insights in pipe flow for thixotropic concretes and fluids in general.

The final expressions for the shear rate profile, velocity profile and the discharge relation can be found in Appendix A. More important are Eq. (22b), Eq. (23) and Eq. (25), because these are rewritten as functions of dimensionless parameters and function variables. This transformation gains more insights and elegance in the thixotropic pipe flow. Alternative dimensionless formulations can be found in Appendix C. The elegance of these formulations facilitates calculation or potential implementation in software. For a start, they also allow to interpret and predict more complicated thixotropic fluids.

Analysis of these dimensionless formulations shows that the pressure number $Pn = \frac{\Delta p R}{2\tau_0 L}$ (or equivalent Bingham number Bn) is the most important dimensionless number of Poiseuille flow of yield stress fluids. The pressure is namely the driving force behind the flow. The thixotropy factor Λ, as well as thixotropy addition ζ, is the ratio of the thixotropic shear scale to the Bingham shear scale. It determines how significant the impact of thixotropy is on the steady-state solution. In addition, Λ is an important parameter in flow start-up or pumping initiation problems.

Moreover, a triangular relation exists between the dimensionless corrected shear stress ε, thixotropy addition ζ and thixotropic projection of the corrected shear stress σ. This thixotropic projection of the shear stress encloses a thixotropy angle ϕ. The thixotropy angle is an indicator of how significant thixotropy is in a pipe flow regime. A thixotropy angle of $\pi/2$ is a predominant thixotropic flow regime, while an angle of 0 is predominantly a Bingham flow regime.

The derived equations are partially derived manually and partially by mathematical software Maple®. The equations are not only validated by a step-by-step verification by this software, but also by a comparison between the solution in which no thixotropy is present and the Buckingham-Reiner equation, which is the solution for a Bingham model.

The shear profiles show that thixotropy has a significant effect on the sheared vs. non-sheared pumping behaviour. The shear rate is a major measure for work that has to be overcome to continue the pumping process. Thixotropy can cause significant increases in required pumping pressures for a constant, controlled pumping flow rate Q. Despite requiring higher pumping pressures or equivalent higher pressure numbers Pn, thixotropy also increases the plug size.

The velocity profiles show that higher thixotropy factors Λ cause an increase in plug radius, and therefore increase the wall shear rate and pressure loss. The transition from plug zone to sheared zone occurs in a non-smooth way, which is not the case for a Bingham or modified Bingham fluid. This is because a non-equilibrium exists in the plug zone, where the internal thixotropic structure continues to grow, while in the sheared zone, an equilibrium structure is achieved by the balance between shear action and thixotropic growth.

The discharge diagram (Figure 7) is an important interpretation and prediction tool for thixotropic pumping. This diagram maps an entire spectrum of Bingham fluids onto a single curve, which can be compared with fluids with different thixotropy levels, characterised by the thixotropy factor Λ. For lower flow rates Q, the thixotropy is more significant on the pipe flow regime, while for higher flow rates, the flow regime asymptotically approaches a pure Bingham flow regime.

Thixotropy can significantly increase the flow initiation pressure, namely by the thixotropy factor Λ compared to a Bingham fluid. This is an important aspect for applied industries with flow start-up problems or pumping interruptions such as the concrete construction industry. Although this finding opposes the work of Wachs et al. [32], in which thixotropic flow start-up is possible for $Pn < 1.0$, this finding still stands. The model of Wachs et al. [32] assumes that structural break-down is predominant and the fluid is compressible, which is possible for waxy crude oils, for example. Therefore a compressive thixotropic structural break-down may allow flow initiation for low pressure numbers below 1. In other applications, structural build-up is important. Hence it is logical that the findings in this work tell otherwise. Indeed, the structural build-up is significant and determines the flow initiation pressure through thixotropy factor Λ. It does not mean that the work of Wachs et al. [32] or this work is invalid. It means that different thixotropy mechanisms are predominant and therefore valid for different thixotropy applications.

Moreover, a potential design point for the pumping operation is defined on these curves. It is called the pumpability contribution point $\widehat{Q}_c$, because it is the point where the contribution in pumping resistance of (thixotropic) yield stress is as much as due to viscous energy dissipation. The viscous contribution of self-compacting concrete is significantly higher than for traditional concrete [23]. To reduce the total pumping resistance, larger pipe diameters are therefore chosen for self-compacting concrete to reduce the viscous contribution.

Lastly, a graph is made to point out the significance of thixotropy, showing how much more pumping pressure would be required relatively compared to a Bingham fluid. For a low discharge Q, higher thixotropy factors Λ require more pumping pressures compared to a Bingham fluid, with a maximum significance of ζ. The lower the thixotropy value Λ, the faster it asymptotically approaches the Bingham solution. The asymptotic approach is an exponential decay, for which a threshold could be defined for which the derived extension can be approximated by the Buckingham-Reiner equation. A similar trend can be observed for the thixotropy angle ϕ_R, which is an alternative interpretation to distinguish thixotropic versus non-thixotropic flow behaviour.

7 Conclusion

In conclusion, a relatively simple, thixotropic Poiseuille flow extension is derived, which is aimed for pumping operations of fresh concrete or cementitious suspensions. The application is not limited to fresh concrete, but could also be used for other thixotropic fluids where the same thixotropic model could be applied, *e.g.* as coatings, paints, inks, clay suspensions, food products, pharmaceutical products, etc. The model may not fully correspond to the underlying thixotropy mechanisms, however, it gives a first indication on how to interpret or predict the pumping operation for these kinds of fluids. As aimed in this work, the dimensionless formulations reveal deeper insights and more elegance for implementation in computational software. The pressure number Pn (or related Bingham number Bn), dimensionless discharge $\widehat{Q}$ and the thixotropy factor Λ are the most important dimensionless numbers characterising the predominance of thixotropic versus non-thixotropic flow regimes. The discharge diagram (Figure 7) is a powerful tool for interpretation and prediction of (non-) thixotropic pumping operations and shows potential for a rheological design of the pumping operation.

The derived extension does not cover the entire range of pumping phenomena occurring during pumping of thixotropic concretes. Neither does it cover the entire time domain, since only a steady-state solution is given. For a transient or time-dependent solution one should solve a partial differential equation, which complicates the purpose of this work. Instead, one could extend this work for instance for alternative, perhaps more complicated, thixotropic models. Moreover, other, non-reversible time-dependent effects could also be included in extension of this work, as long as the complexity of the equations remain to a reasonable level. In fresh concrete for example, hydration also plays a significant role after some time duration [27]. Lastly, one may also extend the Poiseuille flow to more complicated pumping phenomena such as the formation of a so-called lubrication layer and bulk in fresh concrete. In this extension one could consider a thixotropic lubrication layer fluid and a thixotropic bulk fluid.

Acknowledgement: This work is a deliverable of the ERC Advanced Grant project 'SmartCast'. This project has received funding from the European Research Council (ERC) under the European Union's Horizon 2020 research and in-

novation programme (grant agreement No. 693755). This support is gratefully acknowledged.

Bibliography

[1] Barnes HA. Thixotropy - a Review. J Non-Newtonian Fluid Mech. 1997;70(97):1–33. Available from: http://www.sciencedirect.com/science/article/pii/S0377025797000049.

[2] Roussel N. A thixotropy model for fresh fluid concretes: Theory, validation and applications. Cem Concr Res. 2006;36(10):1797–1806. Available from: http://www.sciencedirect.com/science/article/pii/S0008884606001657.

[3] Mewis J, Wagner NJ. Thixotropy. Adv Colloid Interface Sci. 2009;147-148(C):214–227. Available from: http://www.sciencedirect.com/science/article/pii/S0001868608001735.

[4] Roussel N. 11 - Thixotropy: From measurement to casting of concrete. In: Roussel N, editor. Understanding the Rheology of Concrete. Woodhead Publishing Series in Civil and Structural Engineering. Woodhead Publishing; 2012. p. 286–295. Available from: http://www.sciencedirect.com/science/article/pii/B978085709028750011X.

[5] Flatt RJ, Roussel N, Cheeseman CR. Concrete: An eco material that needs to be improved. J Eur Ceram Soc. 2012;32(11):2787–2798. Available from: http://www.sciencedirect.com/science/article/pii/S0955221911005899.

[6] Mujumdar A, Beris AN, Metzner AB. Transient phenomena in thixotropic systems. J Non-Newtonian Fluid Mech. 2002 feb;102(2):157–178. Available from: http://linkinghub.elsevier.com/retrieve/pii/S0377025701001768.

[7] Wallevik JE. Thixotropic investigation on cement paste: Experimental and numerical approach. J Non-Newtonian Fluid Mech. 2005 dec;132(1-3):86–99. Available from: http://linkinghub.elsevier.com/retrieve/pii/S0377025705002314.

[8] Wallevik JE. Rheological properties of cement paste: Thixotropic behavior and structural breakdown. Cem Concr Res. 2009;39(1):14–29. Available from: http://dx.doi.org/10.1016/j.cemconres.2008.10.001.

[9] Banfill PFG. Rheology of Fresh Cement and Concrete. October. The British Society of Rheology; 1991. Available from: http://citeseerx.ist.psu.edu/viewdoc/download?doi=10.1.1.361.7189&rep=rep1&type=pdf.

[10] Chala GT, Sulaiman SA, Japper-Jaafar A. Flow start-up and transportation of waxy crude oil in pipelines-A review. J Non-Newtonian Fluid Mech. 2018;251(November 2017):69–87. Available from: https://doi.org/10.1016/j.jnnfm.2017.11.008.

[11] Papo A. Rheological models for gypsum plaster pastes. Rheol Acta. 1988;27(3):320–325. Available from: http://link.springer.com/10.1007/BF01329748.

[12] Roussel N, Cussigh F. Distinct-layer casting of SCC: The mechanical consequences of thixotropy. Cem Concr Res. 2008;38(5):624–632. Available from: http://www.sciencedirect.com/science/article/pii/S0008884607002426.

[13] Ragouilliaux A, Coussot P, Palermo T, Herzhaft B. Modeling Aging and Yielding of Complex Fluids: Application to an Industrial Material. Oil Gas Sci Technol. 2009;64(5):571–581. Available from: https://doi.org/10.2516/ogst/2009055.

[14] De Schutter G. Thixotropic effects during large-scale concrete pump test on site. In: Santhanam M, Gettu R, Pillai RG, Nayar SK, editors. International Conference on Advances in Construction Materials and Systems. vol. 2. RILEM Publications; 2017. p. 1–7. Available from: http://hdl.handle.net/1854/LU-8615601.

[15] Feys D, Wallevik JE, Yahia A, Khayat KH, Wallevik OH. Extension of the Reiner-Riwlin equation to determine modified Bingham parameters measured in coaxial cylinders rheometers. Mater Struct. 2013;46(1-2):289–311. Available from: http://www.springerlink.com/index/10.1617/s11527-012-9902-6.

[16] Le HD, De Schutter G, Kadri EH, Aggoun S, Vierendeels J, Tichko S, et al. Computational fluid dynamics calibration of Tattersall MK-II type rheometer for concrete. Appl Rheol. 2013;23(3):1–12.

[17] Billingham J, Ferguson JWJ. Laminar, unidirectional flow of a thixotropic fluid in a circular pipe. J Non-Newtonian Fluid Mech. 1993;47(C):21–55.

[18] Ahmadpour A, Sadeghy K. An exact solution for laminar, unidirectional flow of Houska thixotropic fluids in a circular pipe. J Non-Newtonian Fluid Mech. 2013;194:23–31. Available from: http://dx.doi.org/10.1016/j.jnnfm.2012.11.010.

[19] Welty JR, Wicks CE, Wilson RE, Rorrer GL. Fundamentals of Momentum, Heat, and Mass Transfer. 5th ed. John Wiley & Sons Inc; 2007. Available from: https://linkinghub.elsevier.com/retrieve/pii/0017931070900633.

[20] Feys D, Verhoeven R, De Schutter G. Evaluation of time independent rheological models applicable to fresh self-compacting concrete. Appl Rheol. 2007;17(5):1–10.

[21] Feys D. How much is bulk concrete sheared during pumping? Constr Build Mater. 2019;223:341–351. Available from: https://doi.org/10.1016/j.conbuildmat.2019.06.224.

[22] De Schutter G, Feys D. Pumping of Fresh Concrete: Insights and Challenges. RILEM Technical Letters. 2016;1:76. Available from: http://letters.rilem.net/index.php/rilem/article/view/15.

[23] Feys D. 13 – Understanding the pumping of conventional vibtated and self-compacting concrete. In: Roussel N, editor. Understanding the Rheology of Concrete. Woodhead Publishing Series in Civil and Structural Engineering. Woodhead Publishing; 2012. p. 331–353. Available from: http://www.sciencedirect.com/science/article/pii/B9780857090287500133.

[24] Feys D, Verhoeven R, De Schutter G. Extension of the Poiseuille Formula for Shear-thickening Materials and Application to Self-compacting Concrete. Appl Rheol. 2008;18(6):62705–1 – 62705–11. Available from: https://www.degruyter.com/view/journals/arh/18/6/article-p62705-1.xml.

[25] Feys D, Khayat KH, Khatib R. How do concrete rheology, tribology, flow rate and pipe radius influence pumping pressure? Cem Concr Compos. 2016 feb;66:38–46. Available from: https://linkinghub.elsevier.com/retrieve/pii/S0958946515300524.

[26] Tichko S. Hydrodynamic Modelling of the Flow of Self-Compacting Concrete in Formworks [Ph.D. thesis]. Ghent University; 2016. Available from: http://hdl.handle.net/1854/LU-8071379.

[27] Perrot A, Rangeard D, Pierre A. Structural built-up of cement-based materials used for 3D-printing extrusion techniques. Mater Struct. 2016;49(4):1213–1220. Available from: http://dx.doi.org/10.1617/s11527-015-0571-0.

[28] Kaplan D. Pompage des bétons [Ph.D. thesis]. École Nationale des Ponts et Chaussées; 2002. Available from: https://pastel.archives-ouvertes.fr/tel-01310219.

[29] Secrieru E, Cotardo D, Mechtcherine V, Lohaus L, Schröfl C, Begemann C. Changes in concrete properties during pumping and formation of lubricating material under pressure. Cem Concr Res. 2018;108(April):129–139.

[30] Secrieru E, Mohamed W, Fataei S, Mechtcherine V. Assessment and prediction of concrete flow and pumping pressure in pipeline. Cem Concr Compos. 2020;107(November 2019):103495. Available from: https://doi.org/10.1016/j.cemconcomp.2019.103495.

[31] Feys D, Verhoeven R, Schutter GD. Pipe flow velocity profiles of complex suspensions, like concrete. 8th National Congress on Theoretical and Applied Mechanics (NCTAM 2009). 2009;p. 66–73. Available from: https://biblio.ugent.be/publication/967634.

[32] Wachs A, Vinay G, Frigaard I. A 1.5D numerical model for the start up of weakly compressible flow of a viscoplastic and thixotropic fluid in pipelines. J Non-Newtonian Fluid Mech. 2009;159(1-3):81–94. Available from: ttp://www.sciencedirect.com/science/article/pii/S037702570900038X.

[33] Buckingham E. On Plastic Flow through Capillary Tubes. Proc Am Soc Testing Materials. 1921;p. 1154–1156. Available from: https://ci.nii.ac.jp/naid/10011031893/en/.

[34] Feys D. Interactions between rheological properties and pumping of self-compacting concrete [PhD Thesis]. Ghent University; 2009. Available from: http://hdl.handle.net/1854/LU-948561.

[35] Wallevik OH, Wallevik JE. Rheology as a tool in concrete science: The use of rheographs and workability boxes. Cem Concr Res. 2011;41(12):1279–1288. Available from: http://dx.doi.org/10.1016/j.cemconres.2011.01.009.

[36] Jarny S, Roussel N, Rodts S, Bertrand F, Le Roy R, Coussot P. Rheological behavior of cement pastes from MRI velocimetry. Cem Concr Res. 2005;35(10):1873–1881. Available from: http://www.sciencedirect.com/science/article/pii/S0008884605001195.

[37] Ragouilliaux A, Herzhaft B, Ovarlez G, Coussot P. Aging and yielding of colloidal suspension by MRI velocimetry. In: AIP Conference Proceedings. vol. 1027. American Institute of Physics; 2008. p. 1033–1035. Available from: https://doi.org/10.1063/1.2964458.

[38] Coussot P, Tocquer L, Lanos C, Ovarlez G. Macroscopic vs. local rheology of yield stress fluids. J Non-Newtonian Fluid Mech. 2009;158(1-3):85–90.

[39] Le HD. Etude de l'effet de la couche limite sur les profils de vitesses du béton pompé [Ph.D. thesis]. Ghent University; 2014. Available from: http://hdl.handle.net/1854/LU-5941888.

[40] Wiklund J, Stading M. Application of in-line ultrasound Doppler-based UVP-PD rheometry method to concentrated model and industrial suspensions. Flow Meas Instrum. 2008;19(3-4):171–179. Available from: http://www.sciencedirect.com/science/article/pii/S0955598607000908.

[41] Rahman M, Håkansson U, Wiklund J. In-line rheological measurements of cement grouts: Effects of water/cement ratio and hydration. Tunn Undergr Space Technol. 2015;45:34–42. Available from: http://dx.doi.org/10.1016/j.tust.2014.09.003.

[42] Feys D, Verhoeven R, De Schutter G. Fresh self compacting concrete, a shear thickening material. Cem Concr Res. 2008;38(7):920–929. Available from: http://www.sciencedirect.com/science/article/pii/S0008884608000495.

A Partial Derivations

A.1 Partial Derivation of the Velocity Profile

For ease of elaboration, the shear rate relation is written symbolically as follows.

$$\dot{\gamma} = \frac{1}{2\mu}\left[(\tau-\tau_0) + \sqrt{(\tau-\tau_0)^2 - 4\frac{\mu\tau_0}{T\alpha}}\right] \tag{A1a}$$

$$= a\,(B(r) + T(r)) \tag{A1b}$$

Therefore, the velocity profile simplifies to Eq. (A2).

$$v(r) = a\int_r^R B(r)\,dr + a\int_r^R T(r)\,dr \tag{A2}$$

with :

a : $\frac{1}{2\mu}$

$B(r)$: $(\tau-\tau_0)$

$T(r)$: $\sqrt{(\tau-\tau_0)^2 - 4\frac{\mu\tau_0}{T\alpha}}$

In that way the velocity profile results in solving two different integration parts, *i.e.* B as Bingham part and T as thixotropy part.

$$\int_r^R B(r)\,dr = \int_r^R (\tau-\tau_0)\,dr \tag{A3a}$$

$$= \int_r^R \left(\left(\frac{\Delta p}{L}\right)\frac{r}{2}\right)dr \tag{A3b}$$

$$= \int_r^R (br-\delta)\,dr = b\frac{r^2}{2} - \delta r\Big|_r^R \tag{A3c}$$

$$= \left(\frac{\Delta p}{L}\right)\frac{r^2}{4} - \tau_0 r\Big|_r^R \tag{A3d}$$

$$\int_r^R T(r)\,dr = \int_r^R \sqrt{(\tau(r)-\tau_0)^2 - 4\frac{\mu\tau_0}{T\alpha}}\,dr \tag{A4a}$$

$$= \int_r^R \sqrt{\left(\left(\frac{\Delta p}{L}\right)\frac{r}{2} - \tau_0\right)^2 - 4\frac{\mu\tau_0}{T\alpha}}\,dr \tag{A4b}$$

$$= \frac{1}{b}\int_r^R s\,de \tag{A4c}$$

$$= \frac{1}{b}\left(\frac{1}{2}es - \frac{z^2}{2}\ln(e+s)\right)\Big|_r^R \tag{A4d}$$

$$= \frac{1}{b}\left(\frac{1}{2}e\sqrt{e^2-z^2} - \frac{z^2}{2}\ln\left(e+\sqrt{e^2-z^2}\right)\right)\Big|_r^R \tag{A4e}$$

$$= \frac{L}{\Delta p}\left(\left(\frac{\Delta p}{2L}\right)r - \tau_0\right)$$

$$\sqrt{\left(\left(\frac{\Delta p}{2L}\right)r - \tau_0\right)^2 - \sqrt{\frac{4\mu\tau_0}{T\alpha}}^2}\Big|_r^R$$

$$- \frac{L}{\Delta p}z^2\ln\left\{\left(\left(\frac{\Delta p}{2L}\right)r - \tau_0\right)\right.$$

$$\left.\sqrt{\left(\left(\frac{\Delta p}{2L}\right)r - \tau_0\right)^2 - \sqrt{\frac{4\mu\tau_0}{T\alpha}}^2}\right\}\Big|_r^R$$

Combining former partial results, yields the final expression for the velocity profile.

$$v(r) = \frac{1}{2\mu}\left(\left(\frac{\Delta p}{L}\right)\frac{r^2}{4} - \tau_0 r\right)\Big|_r^R \tag{A5}$$

$$+ \frac{1}{2\mu}\frac{L}{\Delta p}\left(\left(\frac{\Delta p}{2L}\right)r - \tau_0\right)\sqrt{\left(\left(\frac{\Delta p}{2L}\right)r - \tau_0\right)^2 - \sqrt{\frac{4\mu\tau_0}{T\alpha}}^2}\Big|_r^R$$

$$- \frac{1}{2\mu}\frac{L}{\Delta p}z^2\ln\left\{\left(\left(\frac{\Delta p}{2L}\right)r - \tau_0\right)\right.$$

$$\left.+ \sqrt{\left(\left(\frac{\Delta p}{2L}\right)r - \tau_0\right)^2 - \sqrt{\frac{4\mu\tau_0}{T\alpha}}^2}\right\}\Big|_r^R$$

The plug velocity $v_{R_{p\Lambda}}$ is explicitly given by the following expression:

$$v_{R_{p\Lambda}} = \frac{1}{2\mu}\left(\left(\frac{\Delta p}{L}\right)\frac{r^2}{4} - \tau_0 r\right)\Big|_{R_{p\Lambda}}^R \tag{A6}$$

$$+ \frac{L}{\Delta p}\left(\left(\frac{\Delta p}{2L}\right)r - \tau_0\right)\sqrt{\left(\left(\frac{\Delta p}{2L}\right)r - \tau_0\right)^2 - \sqrt{\frac{4\mu\tau_0}{T\alpha}}^2}\Big|_{R_{p\Lambda}}^R$$

$$- \frac{L}{\Delta p}z^2\ln\left\{\left(\left(\frac{\Delta p}{2L}\right)r - \tau_0\right)\right.$$

$$\left.+ \sqrt{\left(\left(\frac{\Delta p}{2L}\right)r - \tau_0\right)^2 - \sqrt{\frac{4\mu\tau_0}{T\alpha}}^2}\right\}\Big|_{R_{p\Lambda}}^R$$

with :

δ : τ_0

b : $\left(\frac{\Delta p}{L}\right)\frac{1}{2}$

z : $\sqrt{\frac{4\mu\tau_0}{T\alpha}}$

e : $br - \delta$

s : $\sqrt{e^2 - z^2}$

A.2 Partial Derivation of the Discharge

Substituting Eq. (11) in Eq. (12a), one obtains the following expression, bearing in mind that $r = \frac{1}{b}(e+\delta)$ and $dr = \frac{de}{b}$.

$$Q = \pi R_{p\Lambda}^2 v_{R_{p\Lambda}} + 2\pi\int_{R_{p\Lambda}}^R \left[\, a\left(b\frac{r^2}{2} - \delta r\right)\Big|_r^R \right. \tag{A7a}$$

$$+\frac{a}{2b}es\Big|_r^R-\frac{a}{b}\frac{z^2}{2}\ln(e+s)\Big|_r^R\Bigg]rdr$$
$$=\pi R_{p\Lambda}^2 v_{R_{p\Lambda}}+2\pi a\int_{R_{p\Lambda}}^{R}\left(b\frac{r^2}{2}-\delta r\right)\Big|_r^R rdr \tag{A7b}$$
$$+2\pi\frac{a}{2b^3}\int_{R_{p\Lambda}}^{R}es|_r^R(e+\delta)\,de$$
$$-2\pi\frac{az^2}{2b^3}\int_{R_{p\Lambda}}^{R}\ln(e+s)|_r^R(e+\delta)\,de$$

Yet more elaboration is required to come to a feasible decomposed state that can be easily solved. Therefore the discharge Q is firstly decomposed into a plug part Q_p and a sheared part Q_s. After that, a decomposition of Q_s, is made into a Bingham part Q_{sB} and a thixotropy part Q_{sT}.

$$Q=Q_p+Q_{sB}+Q_{sT} \tag{A8}$$
$$Q_p=\pi R_{p\Lambda}^2 v_{R_{p\Lambda}} \tag{A9}$$
$$Q_{sB}=2\pi a\int_{R_{p\Lambda}}^{R}\left(b\frac{r^2}{2}-\delta r\right)\Big|_r^R rdr \tag{A10}$$
$$Q_{sT}=2\pi\frac{a}{2b^3}\int_{R_{p\Lambda}}^{R}\delta\ es|_r^R\,de+2\pi\frac{a}{2b^3}\int_{R_{p\Lambda}}^{R}es|_r^R\,ede \tag{A11}$$
$$-2\pi\frac{az^2}{2b^3}\int_{R_{p\Lambda}}^{R}\delta\ln(e+s)|_r^R-2\pi\frac{az^2}{2b^3}\int_{R_{p\Lambda}}^{R}\ln(e+s)|_r^R\,ede$$

The shear Bingham part Q_{sB} can easily be retrieved.

$$Q_{sB}=2\pi a\int_{R_{p\Lambda}}^{R}\left(b\frac{r^2}{2}-\delta r\right)\Big|_r^R rdr \tag{A12a}$$
$$=2\pi a\int_{R_{p\Lambda}}^{R}\left(b\frac{r^2}{2}-\delta r\right)\Big|^R rdr \tag{A12b}$$
$$-2\pi a\int_{R_{p\Lambda}}^{R}\left(b\frac{r^3}{2}-\delta r^2\right)dr$$
$$=2\pi a\left(b\frac{R^2}{2}-\delta R\right)\frac{r^2}{2}\Big|_{R_{p\Lambda}}^R \tag{A12c}$$
$$-2\pi a\left(b\frac{r^4}{8}-\delta\frac{r^3}{3}\right)\Big|_{R_{p\Lambda}}^R$$

The thixotropy part Q_{sT} is further unravelled to facilitate the final solution.

$$Q_{sT}=\sum_j^4 Q_{sTj} \tag{A13a}$$

$$Q_{sT1}=2\pi\frac{a}{2b^3}\left(es|^R\int_{R_{p\Lambda}}^{R}\delta de-\int_{R_{p\Lambda}}^{R}\delta esde\right) \tag{A13b}$$
$$Q_{sT2}=2\pi\frac{a}{2b^3}\left(es|^R\int_{R_{p\Lambda}}^{R}ede-\int_{R_{p\Lambda}}^{R}e^2sde\right) \tag{A13c}$$
$$Q_{sT3}=-2\pi\frac{az^2}{2b^3}\left(\ln(e+s)|^R\int_{R_{p\Lambda}}^{R}\delta de\right. \tag{A13d}$$
$$\left.-\int_{R_{p\Lambda}}^{R}\delta\ln(e+s)\,de\right)$$
$$Q_{sT4}=-2\pi\frac{az^2}{2b^3}\left(\ln(e+s)|^R\int_{R_{p\Lambda}}^{R}ede\right. \tag{A13e}$$
$$\left.-\int_{R_{p\Lambda}}^{R}e\ln(e+s)\,de\right)$$

No explicit solution is available yet, but the decomposed parts can be solved one by one. The only remaining unknowns are the solutions of former integrals (Eq. (A13b) to Eq. (A13e)). The solutions of these integrals can be found by the solutions of the primitive functions defined in Appendix B. One finally obtains the following expressions:

$$Q_p=\pi R_{p\Lambda}^2 v_{R_{p\Lambda}} \tag{A14}$$
$$Q_{sB}=2\pi a\left(b\frac{R^2}{2}-\delta R\right)\frac{r^2}{2}\Big|_{R_{p\Lambda}}^R-2\pi a\left(b\frac{r^4}{8}-\delta\frac{r^3}{3}\right)\Big|_{R_{p\Lambda}}^R \tag{A15}$$

$$Q_{sT1}=2\pi\frac{a\delta}{2b^3}\left(es|^R\ e|_{R_{p\Lambda}}^R-\frac{s^3}{3}\Big|_{R_{p\Lambda}}^R\right) \tag{A16a}$$
$$Q_{sT2}=2\pi\frac{a}{2b^3}\left\{es|^R\ \frac{e^2}{2}\Big|_{R_{p\Lambda}}^R+\frac{z^4}{8}\ln(e+s)\Big|_{R_{p\Lambda}}^R\right. \tag{A16b}$$
$$\left.-\frac{es}{8}\left(2e^2-z^2\right)\Big|_{R_{p\Lambda}}^R\right\}$$
$$Q_{sT3}=-2\pi\frac{a\delta z^2}{2b^3}\left\{\ln(e+s)|^R\ e|_{R_{p\Lambda}}^R\right. \tag{A16c}$$
$$\left.-e\ln(e+s)|_{R_{p\Lambda}}^R+s|_{R_{p\Lambda}}^R\right\}$$
$$Q_{sT4}=-2\pi\frac{az^2}{2b^3}\left\{\ln(e+s)|^R\ \frac{e^2}{2}\Big|_{R_{p\Lambda}}^R\right. \tag{A16d}$$
$$\left.-\frac{(2e^2-z^2)}{4}\ln(e+s)\Big|_{R_{p\Lambda}}^R+\frac{es}{4}\Big|_{R_{p\Lambda}}^R\right\}$$

Finally, it is a matter of evaluating and combining explicit Eq. (A14) to Eq. (A16d) for the discharge rate Q, decomposed into the plug discharge part Q_p, the sheared Bingham part Q_{sB} and the sheared thixotropy parts Q_{sT1} to Q_{sT4}.

A.3 Partial Derivation of the Dimensionless Discharge Formulation

To further simplify the decomposed discharge rate (Eq. (A14) to Eq. (A16d)), a transformation is done in order to write these as a function of dimensionless parameters.

$$Q_p = \frac{\pi}{4}\left[\frac{\tau_0 R^3}{\mu}\right]\frac{(1+\zeta)^2}{Pn^3}\left\{Pn^2 - 2Pn + 1 - \zeta^2 + \varepsilon\sigma|^R - \zeta^2 \ln\left(\frac{\varepsilon+\sigma}{\zeta}\right)\Big|^R\right\} \tag{A17}$$

$$Q_{sB} = \frac{\pi}{24}\left[\frac{\tau_0 R^3}{\mu}\right]\frac{1}{Pn^3}\left\{3Pn^4 - 4Pn^3 - 6Pn^2(1+\zeta)^2 + 12Pn(1+\zeta)^2 + (1+\zeta)^3(3\zeta-5)\right\} \tag{A18}$$

$$Q_{sT1} = \frac{\pi}{6}\left[\frac{\tau_0 R^3}{\mu}\right]\frac{1}{Pn^3}\left(3\,\varepsilon^2\sigma|^R - 3\,\varepsilon\sigma|^R\zeta - \sigma^3|^R\right) \tag{A19}$$

$$Q_{sT2} = \frac{\pi}{16}\left[\frac{\tau_0 R^3}{\mu}\right]\frac{1}{Pn^3}\left\{2\varepsilon^3\sigma|^R - 3\zeta^2\,\varepsilon\sigma|^R + \zeta^4 \ln\left(\frac{\varepsilon+\sigma}{\zeta}\right)\Big|^R\right\} \tag{A20}$$

$$Q_{sT3} = \frac{\pi}{2}\left[\frac{\tau_0 R^3}{\mu}\right]\frac{\zeta^2}{Pn^3}\left(\zeta \ln\left(\frac{\varepsilon+\sigma}{\zeta}\right)\Big|^R - \sigma|^R\right) \tag{A21}$$

$$Q_{sT4} = \frac{\pi}{8}\left[\frac{\tau_0 R^3}{\mu}\right]\frac{\zeta^2}{Pn^3}\left(\zeta^2 \ln\left(\frac{\varepsilon+\sigma}{\zeta}\right)\Big|^R - \varepsilon\sigma|^R\right) \tag{A22}$$

Further elaboration and simplification yields the following expressions:

$$Q_p = \frac{\pi}{48}\left[\frac{\tau_0 R^3}{\mu}\right]\frac{(1+\zeta)^2}{Pn^3}\left\{12Pn^2 - 24Pn + 12\left(1-\zeta^2\right) + 12\,\varepsilon\sigma|^R - 12\,\zeta^2 \ln\left(\frac{\varepsilon+\sigma}{\zeta}\right)\Big|^R\right\} \tag{A23}$$

$$Q_{sB} = \frac{\pi}{48}\left[\frac{\tau_0 R^3}{\mu}\right]\frac{1}{Pn^3}\left\{6Pn^4 - 8Pn^3 - 12Pn^2(1+\zeta)^2 + 24Pn(1+\zeta)^2 + 2(1+\zeta)^3(3\zeta-5)\right\} \tag{A24}$$

$$Q_{sT1} = \frac{\pi}{48}\left[\frac{\tau_0 R^3}{\mu}\right]\frac{1}{Pn^3}\left(24\,\varepsilon^2\sigma|^R - 24\,\varepsilon\sigma|^R\zeta - 8\,\sigma^3|^R\right) \tag{A25}$$

$$Q_{sT2} = \frac{\pi}{48}\left[\frac{\tau_0 R^3}{\mu}\right]\frac{1}{Pn^3}\left\{6\varepsilon^3\sigma|^R - 9\zeta^2\,\varepsilon\sigma|^R + 3\zeta^4 \ln\left(\frac{\varepsilon+\sigma}{\zeta}\right)\Big|^R\right\} \tag{A26}$$

$$Q_{sT3} = \frac{\pi}{48}\left[\frac{\tau_0 R^3}{\mu}\right]\frac{1}{Pn^3}\left(24\zeta^3 \ln\left(\frac{\varepsilon+\sigma}{\zeta}\right)\Big|^R - 24\zeta^2\,\sigma|^R\right) \tag{A27}$$

$$Q_{sT4} = \frac{\pi}{48}\left[\frac{\tau_0 R^3}{\mu}\right]\frac{1}{Pn^3}\left(6\zeta^4 \ln\left(\frac{\varepsilon+\sigma}{\zeta}\right)\Big|^R - 6\zeta^2\,\varepsilon\sigma|^R\right) \tag{A28}$$

Finally making the total sum of each discharge part, one obtains the following expression:

$$Q = \frac{\pi}{48}\left[\frac{\tau_0 R^3}{\mu}\right]\frac{1}{Pn^3}\cdot \begin{pmatrix} 6Pn^4 - 8Pn^3 + 2(1+\zeta)^3(1-3\zeta) \\ +\,6\,\varepsilon^3\sigma|^R + 24\,\varepsilon^2\sigma|^R + 3\,\varepsilon\sigma|^R\left(4-\zeta^2\right) \\ -\,24\zeta^2\,\sigma|^R - 8\,\sigma^3|^R \\ -\,3\zeta^2\left(4+\zeta^2\right)\ln\left(\frac{\varepsilon+\sigma}{\zeta}\right)\Big|^R \end{pmatrix} \tag{A29}$$

B Solution of Primitive Functions

All the solutions of the primitive functions can be found in a straightforward way, except the integral of Eq. (B6). For this last integral some manipulation is necessary. The integration constant is omitted for simplicity.

$$F_1 = \int \delta de = \delta e \tag{B1}$$

$$F_2 = \int e de = \frac{e^2}{2} \tag{B2}$$

$$F_3 = \int \delta e s de = \int \delta e \sqrt{e^2 - z^2} de = \frac{\delta s^3}{3} \tag{B3}$$

$$F_4 = \int e^2 s de = \int e^2 \sqrt{e^2 - z^2} de \tag{B4}$$

$$= -\frac{z^4}{8} \ln(e+s) + \frac{es}{8}\left(2e^2 - z^2\right)$$

$$F_5 = \int \delta \ln(e+s)\, de = \int \delta \ln\left(e + \sqrt{e^2 - z^2}\right) de \tag{B5}$$

$$= \delta \left(\ln(e+s)\, e - s\right)$$

$$F_6 = \int e \ln(e+s)\, de = \int e \ln\left(e + \sqrt{e^2 - z^2}\right) de \tag{B6}$$

To solve primitive function F_6, one can make use of partial integration defined by Eq. (B7). Applying partial integration to primitive function F_6, one obtains Eq. (B8e).

$$\int_a^b u \cdot dv = uv|_a^b - \int_a^b v \cdot du \tag{B7}$$

$$F_6 = \int e \ln\left(e + \sqrt{e^2 - z^2}\right) de \tag{B8a}$$

$$= e \cdot \left(e \ln\left(e + \sqrt{e^2 - z^2}\right) - \sqrt{e^2 - z^2}\right) \Big| \tag{B8b}$$

$$- \int \left(e \ln\left(e + \sqrt{e^2 - z^2}\right) - \sqrt{e^2 - z^2}\right) de$$

$$= e \cdot \left(e \ln\left(e + \sqrt{e^2 - z^2}\right) - \sqrt{e^2 - z^2}\right) \tag{B8c}$$

$$- \int e \ln\left(e + \sqrt{e^2 - z^2}\right) de - \int \sqrt{e^2 - z^2} de$$

$$= e \cdot \left(e \ln\left(e + \sqrt{e^2 - z^2}\right) - \sqrt{e^2 - z^2}\right) \tag{B8d}$$

$$- \int e \ln\left(e + \sqrt{e^2 - z^2}\right) de + \frac{e}{2}\sqrt{e^2 - z^2}$$

$$- \frac{z^2}{2} \ln\left(e + \sqrt{e^2 - z^2}\right)$$

$$F_6 = e \cdot \left(e \ln\left(e + \sqrt{e^2 - z^2}\right) - \sqrt{e^2 - z^2}\right) \tag{B8e}$$

$$- F_6 + \frac{e}{2}\sqrt{e^2 - z^2} - \frac{z^2}{2} \ln\left(e + \sqrt{e^2 - z^2}\right)$$

with :

u : e

dv : $\ln\left(e + \sqrt{e^2 - z^2}\right) de$

Solving integral equation Eq. (B8e) eventually results in an explicit solution for primitive function F_6 in Eq. (B9).

$$F_6 = \int e \ln\left(e + \sqrt{e^2 - z^2}\right) de \tag{B9}$$

$$= \frac{\left(2e^2 - z^2\right)}{4} \ln(e+s) - \frac{es}{4}$$

C Alternative Dimensionless Formulations

Due to the mathematical analogy in Eq. (28), the discharge relation can be expressed as a function of a combination of Pn, Λ, ε_R, ζ and ϕ. Hence several expressions can be obtained for the discharge relation, the one more elegant than the other. These alternative expressions are given in this Appendix. To simplify the overall notation, the dimensionless corrected shear stress at the pipe wall $\varepsilon|^R = \varepsilon_R$, it is shortly notated as E. The notation of the thixotropy angle $\phi|^R = \phi_R$ at the pipe wall is also shortly notated as ϕ.

C.1 Formulation as Function of $[Pn, \zeta, \phi]$

$$Q = \frac{\pi}{48}\left[\frac{\tau_0 R^3}{\mu}\right]\frac{1}{Pn^3}\cdot \tag{C1}$$
$$\left(\begin{array}{l} 6Pn^4\,(1+\cos(\phi)) \\ -\,8Pn^3\,\left(1+\cos(\phi)^3\right) \\ -\,3Pn^2\cos(\phi)\left(\zeta^2+8\left(1-\cos(\phi)^2\right)\right) \\ -\,6Pn\cos(\phi)\left(3\zeta^2-4\left(1-\cos(\phi)^2\right)\right) \\ +\,2\,(1+\zeta)^3\,(1-3\zeta) \\ +\,\cos(\phi)\left(21\zeta^2-6+8\cos(\phi)^2\right) \\ -\,3\zeta^2\left(4+\zeta^2\right)\ln\left(\dfrac{Pn-1}{\zeta}\,(\cos(\phi)+1)\right) \end{array}\right)$$

C.2 Formulation as Function of $[E, \zeta, \phi]$

$$Q = \frac{\pi}{48}\left[\frac{\tau_0 R^3}{\mu}\right](E-1)^{-3}\cdot \tag{C2}$$
$$\left(\begin{array}{l} 6E^4\,(\cos(\phi)+1) \\ +\,8E^3\left(\cos(\phi)\left(-\cos(\phi)^2+3\right)+2\right) \\ +\,3E^2\left(\cos(\phi)\left(4-\zeta^2\right)+4\right) \\ -\,24E\cos(\phi)\,\zeta^2 \\ -\,2\zeta^2\left(3\zeta^2+8\zeta+4\right) \\ -\,3\zeta^2\left(4+\zeta^2\right)\ln\left(\dfrac{E}{\zeta}\,(\cos(\phi)+1)\right) \end{array}\right)$$

C.3 Formulation as Function of $[Pn, \Lambda, \phi]$

$$Q = \frac{\pi}{48}\left[\frac{\tau_0 R^3}{\mu}\right]\frac{1}{Pn^3}\cdot \tag{C3}$$
$$\left(\begin{array}{l} 6Pn^4\,(\cos(\phi)+3) \\ -\,8Pn^3\,(\cos(\phi)+3\Lambda+4) \\ +\,3Pn^2\left(\cos(\phi)\left(8\cos(\phi)^2-\Lambda^2+2\Lambda-9\right)+4\Lambda\,(\Lambda+4)\right) \\ +\,6Pn\left(\cos(\phi)\left(-4\cos(\phi)^2-3\Lambda^2+6\Lambda+2\right)-4\right) \\ +\,\cos(\phi)\left(8\cos(\phi)^2+21\Lambda^2-42\Lambda+15\right) \\ +\,2\Lambda^3\,(-3\Lambda+4) \\ -\,3\,(\Lambda-1)^2\left(\Lambda^2-2\Lambda+5\right)\ln\left(\dfrac{Pn-1}{\Lambda-1}\,(\cos(\phi)+1)\right) \end{array}\right)$$

D Poiseuille Flow Extensions for the Modified Bingham Model

The analytical solution for the modified Bingham model was developed by Feys et al. [31]. Reformulation as a function of dimensionless parameters yields the following expressions. Herein is MBn the modified Bingham number.

$$\dot{\gamma}(r) = 2\left[\frac{\tau_0}{\mu}\right] MBn^{-1}(\chi - 1) \tag{C4a}$$

$$v(r) = \frac{2}{3}\left[\frac{\tau_0 R}{\mu}\right] MBn^{-2}Pn^{-1}\left(\chi^2(2\chi - 3)\right)\Big|_r^R \tag{C4b}$$

$$Q = \frac{2\pi}{105}\left[\frac{\tau_0 R^3}{\mu}\right] MBn^{-4}Pn^{-3} \tag{C4c}$$

$$\begin{pmatrix} 16(\omega - 1) \\ + 4MBn(-\omega Pn + (7 - 6\omega)) \\ + 2MBn^2\left(3Pn^2 + 8Pn + (24\omega - 35)\right) \\ + MBn^3\left(5Pn^3(6\omega - 7) - 6\omega Pn^2\right) \\ + MBn^3(-8\omega Pn + (35 - 16\omega)) \end{pmatrix}$$

with :

MBn : $\frac{4c\tau_0}{\mu^2}$

$\chi(r)$: $\sqrt{1 + MBn\left(Pn\frac{r}{R} - 1\right)}$

$\omega = \chi|^R$: $\sqrt{1 + MBn(Pn - 1)}$

E Discharge Tables

In this Appendix, a brief summary is given of numerical values computed for the discharge relation for various values of thixotropy factor Λ. It is applicable for potential future use to predict thixotropic concrete pumping, but not limited to it. The values for a thixotropy factor Λ of 1.0 (Table E3) correspond to the Buckingham-Reiner solution which can also serve in practice. This is namely the solution for a non-thixotropic Bingham fluid.

Table E3 through Table E7 depict the pressure loss number Pn (equivalent to the dimensionless wall shear stress $\widehat{\tau}_R$), thixotropy angle ϕ_R, dimensionless plug velocity $\widehat{v}_{R_{p\Lambda}}$, the dimensionless wall shear rate $\widehat{\dot{\gamma}}_R$ as well as other useful dimensionless numbers as a function of the dimensionless discharge $\widehat{Q}$.

Table E3: Brief summary of numerical values of the discharge relations shown in Figure 7 for a thixotropy factor $\Lambda = 1.0$.

$\Lambda = 1.0$							
$\widehat{Q}$ [-]	Pn [-]	ε_R [-]	σ_R [-]	ϕ_R [rad]	ϕ_R [°]	$\widehat{\dot{\gamma}}_R$ [-]	$\widehat{v}_{R_{p\Lambda}}$ [-]
0	1.00	0.00	0.00	1.57	90.0	0.00	0.00
0.2	1.49	0.49	0.49	0.00	0.0	0.49	0.08
0.4	1.78	0.78	0.78	0.00	0.0	0.78	0.17
0.6	2.06	1.06	1.06	0.00	0.0	1.06	0.27
0.8	2.33	1.33	1.33	0.00	0.0	1.33	0.38
1	2.59	1.59	1.59	0.00	0.0	1.59	0.49
1.2	2.85	1.85	1.85	0.00	0.0	1.85	0.60
1.4	3.10	2.10	2.10	0.00	0.0	2.10	0.71
1.6	3.36	2.36	2.36	0.00	0.0	2.36	0.83
1.8	3.62	2.62	2.62	0.00	0.0	2.62	0.95
2	3.87	2.87	2.87	0.00	0.0	2.87	1.07
2.2	4.13	3.13	3.13	0.00	0.0	3.13	1.19
2.4	4.39	3.39	3.39	0.00	0.0	3.39	1.31
2.6	4.64	3.64	3.64	0.00	0.0	3.64	1.43
2.8	4.90	3.90	3.90	0.00	0.0	3.90	1.55
3	5.15	4.15	4.15	0.00	0.0	4.15	1.67
3.2	5.41	4.41	4.41	0.00	0.0	4.41	1.80
3.4	5.66	4.66	4.66	0.00	0.0	4.66	1.92
3.6	5.92	4.92	4.92	0.00	0.0	4.92	2.04
3.8	6.17	5.17	5.17	0.00	0.0	5.17	2.17
4	6.43	5.43	5.43	0.00	0.0	5.43	2.29
4.2	6.68	5.68	5.68	0.00	0.0	5.68	2.41
4.4	6.93	5.93	5.93	0.00	0.0	5.93	2.54
4.6	7.19	6.19	6.19	0.00	0.0	6.19	2.66
4.8	7.44	6.44	6.44	0.00	0.0	6.44	2.79
5	7.70	6.70	6.70	0.00	0.0	6.70	2.91
5.2	7.95	6.95	6.95	0.00	0.0	6.95	3.04
5.4	8.21	7.21	7.21	0.00	0.0	7.21	3.17
5.6	8.46	7.46	7.46	0.00	0.0	7.46	3.29
5.8	8.72	7.72	7.72	0.00	0.0	7.72	3.42
6	8.97	7.97	7.97	0.00	0.0	7.97	3.54
6.2	9.23	8.23	8.23	0.00	0.0	8.23	3.67
6.4	9.48	8.48	8.48	0.00	0.0	8.48	3.79
6.6	9.74	8.74	8.74	0.00	0.0	8.74	3.92
6.8	9.99	8.99	8.99	0.00	0.0	8.99	4.05
7	10.25	9.25	9.25	0.00	0.0	9.25	4.17
7.2	10.50	9.50	9.50	0.00	0.0	9.50	4.30
7.4	10.76	9.76	9.76	0.00	0.0	9.76	4.42
7.6	11.01	10.01	10.01	0.00	0.0	10.01	4.55
7.8	11.26	10.26	10.26	0.00	0.0	10.26	4.68
8	11.52	10.52	10.52	0.00	0.0	10.52	4.80
8.2	11.77	10.77	10.77	0.00	0.0	10.77	4.93
8.4	12.03	11.03	11.03	0.00	0.0	11.03	5.06
8.6	12.28	11.28	11.28	0.00	0.0	11.28	5.18
8.8	12.54	11.54	11.54	0.00	0.0	11.54	5.31
9	12.79	11.79	11.79	0.00	0.0	11.79	5.44
9.2	13.05	12.05	12.05	0.00	0.0	12.05	5.56
9.4	13.30	12.30	12.30	0.00	0.0	12.30	5.69
9.6	13.56	12.56	12.56	0.00	0.0	12.56	5.82
9.8	13.81	12.81	12.81	0.00	0.0	12.81	5.94
10	14.07	13.07	13.07	0.00	0.0	13.07	6.07

Table E4: Brief summary of numerical values of the discharge relations shown in Figure 7 for a thixotropy factor $\Lambda = 2.0$.

$\Lambda = 2.0$							
$\widehat{Q}$ [-]	Pn [-]	ε_R [-]	σ_R [-]	ϕ_R [rad]	ϕ_R [°]	$\widehat{\dot{\gamma}}_R$ [-]	$\widehat{v}_{R_{p\Lambda}}$ [-]
0	2.00	1.00	0.00	1.57	90.0	0.50	0.00
0.2	2.20	1.20	0.66	0.77	44.1	0.93	0.07
0.4	2.39	1.39	0.96	0.55	31.2	1.18	0.15
0.6	2.58	1.58	1.23	0.41	23.5	1.41	0.23
0.8	2.78	1.78	1.48	0.32	18.3	1.63	0.33
1	2.99	1.99	1.72	0.25	14.6	1.86	0.43
1.2	3.21	2.21	1.97	0.21	11.9	2.09	0.53
1.4	3.43	2.43	2.21	0.17	9.8	2.32	0.64
1.6	3.65	2.65	2.45	0.14	8.2	2.55	0.75
1.8	3.88	2.88	2.70	0.12	6.9	2.79	0.86
2	4.11	3.11	2.95	0.10	5.9	3.03	0.98
2.2	4.35	3.35	3.19	0.09	5.1	3.27	1.09
2.4	4.58	3.58	3.44	0.08	4.5	3.51	1.21
2.6	4.82	3.82	3.69	0.07	3.9	3.76	1.33
2.8	5.07	4.07	3.94	0.06	3.5	4.00	1.45
3	5.31	4.31	4.19	0.05	3.1	4.25	1.58
3.2	5.55	4.55	4.44	0.05	2.8	4.50	1.70
3.4	5.80	4.80	4.69	0.04	2.5	4.75	1.82
3.6	6.05	5.05	4.95	0.04	2.3	5.00	1.95
3.8	6.29	5.29	5.20	0.04	2.0	5.25	2.07
4	6.54	5.54	5.45	0.03	1.9	5.50	2.20
4.2	6.79	5.79	5.70	0.03	1.7	5.75	2.32
4.4	7.04	6.04	5.96	0.03	1.6	6.00	2.45
4.6	7.29	6.29	6.21	0.03	1.4	6.25	2.58
4.8	7.54	6.54	6.46	0.02	1.3	6.50	2.70
5	7.79	6.79	6.72	0.02	1.2	6.75	2.83
5.2	8.04	7.04	6.97	0.02	1.2	7.01	2.95
5.4	8.29	7.29	7.22	0.02	1.1	7.26	3.08
5.6	8.54	7.54	7.48	0.02	1.0	7.51	3.21
5.8	8.79	7.79	7.73	0.02	0.9	7.76	3.33
6	9.05	8.05	7.98	0.02	0.9	8.02	3.46
6.2	9.30	8.30	8.24	0.01	0.8	8.27	3.59
6.4	9.55	8.55	8.49	0.01	0.8	8.52	3.71
6.6	9.80	8.80	8.75	0.01	0.7	8.77	3.84
6.8	10.06	9.06	9.00	0.01	0.7	9.03	3.97
7	10.31	9.31	9.25	0.01	0.7	9.28	4.10
7.2	10.56	9.56	9.51	0.01	0.6	9.54	4.22
7.4	10.81	9.81	9.76	0.01	0.6	9.79	4.35
7.6	11.07	10.07	10.02	0.01	0.6	10.04	4.48
7.8	11.32	10.32	10.27	0.01	0.5	10.30	4.60
8	11.57	10.57	10.53	0.01	0.5	10.55	4.73
8.2	11.83	10.83	10.78	0.01	0.5	10.80	4.86
8.4	12.08	11.08	11.03	0.01	0.5	11.06	4.99
8.6	12.33	11.33	11.29	0.01	0.4	11.31	5.11
8.8	12.59	11.59	11.54	0.01	0.4	11.56	5.24
9	12.84	11.84	11.80	0.01	0.4	11.82	5.37
9.2	13.09	12.09	12.05	0.01	0.4	12.07	5.50
9.4	13.35	12.35	12.31	0.01	0.4	12.33	5.62
9.6	13.60	12.60	12.56	0.01	0.4	12.58	5.75
9.8	13.85	12.85	12.82	0.01	0.3	12.83	5.88
10	14.11	13.11	13.07	0.01	0.3	13.09	6.01

Table E5: Brief summary of numerical values of the discharge relations shown in Figure 7 for a thixotropy factor $\Lambda = 3.0$.

$\Lambda = 3.0$							
$\widehat{Q}$ [-]	Pn [-]	ε_R [-]	σ_R [-]	ϕ_R [rad]	ϕ_R [°]	$\widehat{\dot{\gamma}}_R$ [-]	$\widehat{v}_{R_{p\Lambda}}$ [-]
0	3.00	2.00	0.00	1.57	90.0	1.00	0.00
0.2	3.16	2.16	0.82	1.03	58.9	1.49	0.07
0.4	3.32	2.32	1.17	0.84	48.2	1.74	0.14
0.6	3.47	2.47	1.45	0.71	40.9	1.96	0.22
0.8	3.63	2.63	1.71	0.61	35.2	2.17	0.30
1	3.80	2.80	1.96	0.53	30.7	2.38	0.39
1.2	3.97	2.97	2.20	0.47	26.9	2.59	0.48
1.4	4.15	3.15	2.44	0.41	23.7	2.79	0.57
1.6	4.34	3.34	2.67	0.37	21.1	3.00	0.67
1.8	4.53	3.53	2.90	0.33	18.8	3.22	0.77
2	4.72	3.72	3.14	0.29	16.8	3.43	0.88
2.2	4.92	3.92	3.37	0.26	15.1	3.65	0.99
2.4	5.13	4.13	3.61	0.24	13.6	3.87	1.10
2.6	5.34	4.34	3.85	0.21	12.3	4.09	1.21
2.8	5.55	4.55	4.09	0.19	11.1	4.32	1.33
3	5.77	4.77	4.33	0.18	10.1	4.55	1.44
3.2	5.99	4.99	4.57	0.16	9.3	4.78	1.56
3.4	6.21	5.21	4.81	0.15	8.5	5.01	1.68
3.6	6.43	5.43	5.05	0.14	7.8	5.24	1.80
3.8	6.66	5.66	5.30	0.13	7.2	5.48	1.92
4	6.89	5.89	5.54	0.12	6.6	5.72	2.05
4.2	7.12	6.12	5.79	0.11	6.1	5.96	2.17
4.4	7.36	6.36	6.04	0.10	5.7	6.20	2.29
4.6	7.59	6.59	6.28	0.09	5.3	6.44	2.42
4.8	7.83	6.83	6.53	0.09	4.9	6.68	2.54
5	8.07	7.07	6.78	0.08	4.6	6.92	2.67
5.2	8.31	7.31	7.03	0.07	4.3	7.17	2.80
5.4	8.55	7.55	7.28	0.07	4.0	7.41	2.92
5.6	8.79	7.79	7.53	0.07	3.8	7.66	3.05
5.8	9.03	8.03	7.78	0.06	3.6	7.91	3.18
6	9.28	8.28	8.03	0.06	3.3	8.15	3.30
6.2	9.52	8.52	8.28	0.06	3.2	8.40	3.43
6.4	9.77	8.77	8.53	0.05	3.0	8.65	3.56
6.6	10.01	9.01	8.79	0.05	2.8	8.90	3.69
6.8	10.26	9.26	9.04	0.05	2.7	9.15	3.81
7	10.50	9.50	9.29	0.04	2.5	9.40	3.94
7.2	10.75	9.75	9.54	0.04	2.4	9.65	4.07
7.4	11.00	10.00	9.79	0.04	2.3	9.90	4.20
7.6	11.24	10.24	10.05	0.04	2.2	10.15	4.33
7.8	11.49	10.49	10.30	0.04	2.1	10.40	4.45
8	11.74	10.74	10.55	0.03	2.0	10.65	4.58
8.2	11.99	10.99	10.81	0.03	1.9	10.90	4.71
8.4	12.24	11.24	11.06	0.03	1.8	11.15	4.84
8.6	12.49	11.49	11.31	0.03	1.7	11.40	4.97
8.8	12.74	11.74	11.57	0.03	1.7	11.65	5.10
9	12.99	11.99	11.82	0.03	1.6	11.90	5.23
9.2	13.24	12.24	12.07	0.03	1.5	12.15	5.35
9.4	13.49	12.49	12.33	0.03	1.5	12.41	5.48
9.6	13.74	12.74	12.58	0.02	1.4	12.66	5.61
9.8	13.99	12.99	12.83	0.02	1.4	12.91	5.74
10	14.24	13.24	13.09	0.02	1.3	13.16	5.87

Table E6: Brief summary of numerical values of the discharge relations shown in Figure 7 for a thixotropy factor $\Lambda = 4.0$.

$\Lambda = 4.0$							
$\widehat{Q}$ [-]	Pn [-]	ε_R [-]	σ_R [-]	ϕ_R [rad]	ϕ_R [°]	$\widehat{\dot{\gamma}}_R$ [-]	$\widehat{v}_{R_{p\Lambda}}$ [-]
0	4.00	3.00	0.00	1.57	90.0	1.50	0.00
0.2	4.15	3.15	0.95	1.14	65.3	2.05	0.07
0.4	4.29	3.29	1.35	0.98	56.3	2.32	0.14
0.6	4.43	3.43	1.66	0.87	49.9	2.55	0.21
0.8	4.57	3.57	1.94	0.78	44.8	2.76	0.29
1	4.72	3.72	2.20	0.71	40.5	2.96	0.37
1.2	4.87	3.87	2.45	0.64	36.8	3.16	0.45
1.4	5.03	4.03	2.69	0.59	33.6	3.36	0.54
1.6	5.19	4.19	2.93	0.54	30.8	3.56	0.63
1.8	5.36	4.36	3.16	0.49	28.3	3.76	0.72
2	5.53	4.53	3.39	0.46	26.1	3.96	0.82
2.2	5.70	4.70	3.62	0.42	24.0	4.16	0.92
2.4	5.88	4.88	3.85	0.39	22.2	4.36	1.02
2.6	6.06	5.06	4.08	0.36	20.6	4.57	1.12
2.8	6.25	5.25	4.31	0.33	19.1	4.78	1.23
3	6.44	5.44	4.54	0.31	17.7	4.99	1.34
3.2	6.63	5.63	4.77	0.29	16.5	5.20	1.45
3.4	6.83	5.83	5.00	0.27	15.3	5.42	1.56
3.6	7.03	6.03	5.24	0.25	14.3	5.64	1.67
3.8	7.24	6.24	5.47	0.23	13.4	5.86	1.79
4	7.45	6.45	5.71	0.22	12.5	6.08	1.91
4.2	7.66	6.66	5.95	0.20	11.7	6.30	2.02
4.4	7.87	6.87	6.18	0.19	11.0	6.53	2.14
4.6	8.09	7.09	6.42	0.18	10.3	6.76	2.26
4.8	8.31	7.31	6.67	0.17	9.7	6.99	2.39
5	8.53	7.53	6.91	0.16	9.1	7.22	2.51
5.2	8.75	7.75	7.15	0.15	8.6	7.45	2.63
5.4	8.98	7.98	7.39	0.14	8.1	7.69	2.76
5.6	9.21	8.21	7.64	0.13	7.7	7.92	2.88
5.8	9.43	8.43	7.88	0.13	7.3	8.16	3.00
6	9.66	8.66	8.13	0.12	6.9	8.40	3.13
6.2	9.90	8.90	8.37	0.11	6.5	8.64	3.26
6.4	10.13	9.13	8.62	0.11	6.2	8.87	3.38
6.6	10.36	9.36	8.87	0.10	5.9	9.12	3.51
6.8	10.60	9.60	9.12	0.10	5.6	9.36	3.64
7	10.83	9.83	9.36	0.09	5.3	9.60	3.76
7.2	11.07	10.07	9.61	0.09	5.1	9.84	3.89
7.4	11.31	10.31	9.86	0.08	4.9	10.09	4.02
7.6	11.55	10.55	10.11	0.08	4.6	10.33	4.15
7.8	11.79	10.79	10.36	0.08	4.4	10.57	4.27
8	12.03	11.03	10.61	0.07	4.2	10.82	4.40
8.2	12.27	11.27	10.86	0.07	4.1	11.07	4.53
8.4	12.51	11.51	11.11	0.07	3.9	11.31	4.66
8.6	12.75	11.75	11.36	0.07	3.7	11.56	4.79
8.8	13.00	12.00	11.61	0.06	3.6	11.81	4.92
9	13.24	12.24	11.87	0.06	3.4	12.05	5.05
9.2	13.48	12.48	12.12	0.06	3.3	12.30	5.18
9.4	13.73	12.73	12.37	0.06	3.2	12.55	5.31
9.6	13.97	12.97	12.62	0.05	3.1	12.80	5.43
9.8	14.22	13.22	12.87	0.05	3.0	13.05	5.56
10	14.46	13.46	13.12	0.05	2.8	13.29	5.69

Table E7: Brief summary of numerical values of the discharge relations shown in Figure 7 for a thixotropy factor $\Lambda = 5.0$.

$\Lambda = 5.0$							
$\widehat{Q}$ [-]	Pn [-]	ε_R [-]	σ_R [-]	ϕ_R [rad]	ϕ_R [°]	$\widehat{\dot{\gamma}}_R$ [-]	$\widehat{v}_{R_{p\Lambda}}$ [-]
0	5.00	4.00	0.00	1.57	90.0	2.00	0.00
0.2	5.14	4.14	1.07	1.20	68.9	2.61	0.07
0.4	5.27	4.27	1.51	1.07	61.1	2.89	0.13
0.6	5.41	4.41	1.85	0.97	55.4	3.13	0.21
0.8	5.54	4.54	2.16	0.89	50.8	3.35	0.28
1	5.68	4.68	2.43	0.82	46.9	3.56	0.36
1.2	5.82	4.82	2.69	0.76	43.5	3.76	0.44
1.4	5.97	4.97	2.94	0.71	40.5	3.95	0.52
1.6	6.11	5.11	3.18	0.66	37.7	4.15	0.60
1.8	6.26	5.26	3.42	0.62	35.3	4.34	0.69
2	6.42	5.42	3.65	0.58	33.0	4.53	0.78
2.2	6.57	5.57	3.88	0.54	31.0	4.73	0.87
2.4	6.74	5.74	4.11	0.51	29.1	4.92	0.97
2.6	6.90	5.90	4.34	0.48	27.4	5.12	1.06
2.8	7.07	6.07	4.56	0.45	25.7	5.32	1.16
3	7.24	6.24	4.79	0.42	24.3	5.52	1.26
3.2	7.42	6.42	5.02	0.40	22.9	5.72	1.37
3.4	7.60	6.60	5.24	0.38	21.6	5.92	1.47
3.6	7.78	6.78	5.47	0.36	20.4	6.13	1.58
3.8	7.96	6.96	5.70	0.34	19.3	6.33	1.69
4	8.15	7.15	5.93	0.32	18.2	6.54	1.80
4.2	8.35	7.35	6.16	0.30	17.2	6.75	1.91
4.4	8.54	7.54	6.39	0.29	16.3	6.97	2.02
4.6	8.74	7.74	6.62	0.27	15.5	7.18	2.14
4.8	8.94	7.94	6.86	0.26	14.7	7.40	2.25
5	9.14	8.14	7.09	0.24	14.0	7.62	2.37
5.2	9.35	8.35	7.33	0.23	13.3	7.84	2.49
5.4	9.56	8.56	7.56	0.22	12.6	8.06	2.61
5.6	9.77	8.77	7.80	0.21	12.0	8.29	2.73
5.8	9.98	8.98	8.04	0.20	11.4	8.51	2.85
6	10.20	9.20	8.28	0.19	10.9	8.74	2.97
6.2	10.41	9.41	8.52	0.18	10.4	8.97	3.09
6.4	10.63	9.63	8.76	0.17	9.9	9.20	3.22
6.6	10.85	9.85	9.00	0.17	9.5	9.43	3.34
6.8	11.07	10.07	9.24	0.16	9.1	9.66	3.46
7	11.30	10.30	9.49	0.15	8.7	9.89	3.59
7.2	11.52	10.52	9.73	0.15	8.3	10.13	3.71
7.4	11.75	10.75	9.98	0.14	8.0	10.36	3.84
7.6	11.98	10.98	10.22	0.13	7.6	10.60	3.97
7.8	12.20	11.20	10.47	0.13	7.3	10.83	4.09
8	12.43	11.43	10.71	0.12	7.0	11.07	4.22
8.2	12.67	11.67	10.96	0.12	6.8	11.31	4.35
8.4	12.90	11.90	11.20	0.11	6.5	11.55	4.47
8.6	13.13	12.13	11.45	0.11	6.2	11.79	4.60
8.8	13.36	12.36	11.70	0.10	6.0	12.03	4.73
9	13.60	12.60	11.95	0.10	5.8	12.27	4.86
9.2	13.84	12.84	12.20	0.10	5.6	12.52	4.99
9.4	14.07	13.07	12.44	0.09	5.4	12.76	5.11
9.6	14.31	13.31	12.69	0.09	5.2	13.00	5.24
9.8	14.55	13.55	12.94	0.09	5.0	13.24	5.37
10	14.79	13.79	13.19	0.08	4.8	13.49	5.50